Univerzita Karlova v Praze

Přírodovědecká fakulta

BAKALÁŘSKÁ PRÁCE

Dominika Zákutná

Příprava a vlastnosti nanočástic chromitů

Katedra anorganické chemie

Vedoucí bakalářské práce:	RNDr. Daniel Nižňanský, Ph.D.
Konzultant:	RNDr. Jana Vejpravová, Ph.D.
Studijní program:	Chemie v přírodních vědách

2013

Charles University in Prague

Faculty of Science

BACHELOR`S THESIS

Dominika Zákutná

Preparation and characterization of chromite nanoparticles

Department of Inorganic Chemistry

Supervisor:	RNDr. Daniel Nižňanský, Ph.D.
Consultant:	RNDr. Jana Vejpravová, Ph.D.
Study program:	Chemistry in science

2013

Tato bakalářská práce byla podpořena Grantovou Agenturou České Republiky pod projektem č. P108/10/1250 a s dlouhodobým řešením výzkumného záměru MSM0021620857.

Prohlašuji, že jsem tuto bakalářskou práci vypracovala samostatně pod vedením školitele RNDr. Daniela Nižňanského, Ph.D. a RNDr. Jany Vejpravové že jsem uvedla všechny použité informační zdroje a literaturu.

Jsem si vědoma toho, že případné využití výsledků, získaných v této práci, mimo Univerzitu Karlovu v Praze je možné pouze po písemném souhlasu této univerzity.

V Praze dne 22.dubna 2013 Dominika Zákutná

This work was supported by the Grant Agency of the Czech Republic under project no. P108/10/1250 and by the Long Term Research Plan of the Ministry of Education of the Czech Republic (MSM0021620857).

I declare that I prepared the bachelor`s thesis individually, under supervision of RNDr. Daniel Nižňanský, PhD and RNDr. Jana Vejpravová, PhD and that I properly cited all used information and literary sources.

I am aware that any use of the results obtained in this work outside the Charles University in Prague is possible only with the written consent of the University.

In Prague 22.4.2013 Dominika Zákutná

I would like to thank to my supervisor RNDr. Daniel Nižňanský, Ph.D. for his professional and technical support and patience. I would like also to thank to RNDr. Jana Vejpravová, Ph.D., group leader of MNS (Magnetic NanoSystems) of the Institute of Physics of the Academy of Science of Czech Republic, for magnetic properties measurements and for the explanation of the theory of magnetism, Mgr. Anton Repko for the explanation of hydrothermal synthesis.

My gratitude also includes Carla Cannas and Andrea Ardu from Universita di Cagliari in Italy for TEM and HRTEM studies of my samples.

I thanks also to other members of the MNS group for their help in the processing of data, Vlastimila Pitterová for X-Ray diffraction measurements and RNDr. Irena Matulková, PhD. for Raman spectra measurements.

Název práce: Příprava a vlastnosti nanočástic chromitů

Autor: Dominika Zákutná

Katedra: Katedra anorganické chemie, PřF UK Praha

Vedoucí bakalářské práce: RNDr. Daniel Nižňanský, PhD.

Konzultant: RNDr. Jana Vejpravová, PhD.

e-mail vedoucího: niznansk@natur.cuni.cz

Abstrakt:

Tato práce se zabývá hydrotermální přípravou nanočástic oxidu kobaltnato-chromitého ($CoCr_2O_4$ NPs), jejich charakterizací a studiem jejich magnetických vlastností. Při přípravě se vycházelo z příslušných chloridů v prostředí voda-ethanol-kyselina olejová. Vzorky byly charakterizovány pomocí práškové rentgenové difrakce (PXRD), transmisní a vysokorozlišovací transmisní elektronové mikroskopie (TEM, HRTEM), skenovací elektronové mikroskopie (SEM), Ramanovy a infračervené spektroskopie a magnetickým měřením závislosti magnetizace na teplotě a poli. Bylo zjištěno, že teplota furkace, T_f, je závislá na velikosti částic.

Klíčová slova: $CoCr_2O_4$, systém jako super spinové sklo, hydrotermální metoda, magnetické vlastnosti, oleáty.

Title:	Preparation and Characterization of Chromites nanoparticles
Author:	Dominika Zákutná
Department:	Department of Inorganic Chemistry, Faculty of Science, Charles University of Prague
Supervisor:	RNDr. Daniel Nižňanský, Ph.D.
Consultant:	RNDr. Jana Vejpravová, Ph.D.
Supervisor`s e-mail address:	niznansk@natur.cuni.cz

Abstract:

This work concerns the hydrothermal preparation of cobalt chromite nanoparticles ($CoCr_2O_4$), their characterization and the study of their magnetic properties. The preparation is based on the chlorides in the water-ethanol-oleic acid system. The samples were characterized by Powder X-ray Diffraction (PXRD), Transmission and High Resolution Electron Microscopy (TEM, HRTEM), Scanning Electron Microscopy (SEM), Raman and Infrared Spectroscopy and magnetic measurements of magnetization as a function of temperature and field. It was found, that furcation temperature, T_f depends on particle size.

Keywords: $CoCr_2O_4$, superspin-glass like system, hydrothermal method, magnetic properties, oleates

Contents

Chapter 1

Introduction

In the last years, the materials research is oriented to the nanoscale materials. The nanomaterials are interesting field of study because they show different physical and chemical properties in comparison with their bulk analogues. The reason for this behaviour is an increased relative surface area and quantum phenomena effects that play the roles in the given dimension of the nanomaterials and they influence their physical and chemical behaviour. The phenomena depending on the dimension of the materials result from the quantum restrictions on movement of electrons in the confined direction, while surface effects have their origin in the increased ratio of surface atoms and in the crystal lattice symmetry disorder at the border of nanostructures, leading to an increase of surface anisotropy, disorder of magnetic moments at the surface, spin frustration and magnetic interactions weakening. The tailoring of nanostructured magnetic materials permits the control of interparticle interactions, defects and vacancies.

Magnetic nanoparticles represent the attractive field due to their wide potential application and tuneable properties. Small superparamagnetic particles can be used for various biomedical applications ranging from drug delivery, cancer diagnostic and treatment, to various *in vitro* labelling and separation. Larger particles could be used for information storage and for electronic devices.

The preparation of nanoscale objects can be accomplished by either physical methods or chemical synthetic routes. Older routes of preparation are based mainly on coprecipitation, but these methods suffer from poor size distribution, aggregation and low crystallinity. Some of these problems are resolved by reverse micelle approach. At the present time, current development is focused on high temperature decomposition in organic solvents. This method leads to the isolated magnetic nanoparticles having good crystallinity and very narrow crystal size distribution[1]. However, this method is not very friendly for environment due to toxic organic solvents and by products, which are difficult to remove from the prepared nanoparticles. This problem can be resolved by using of hydrothermal method, which

represents the successful way for preparation of various types of materials (precious metals, dielectric, magnetic, semiconductor, luminescent)[2]. The nanoparticles prepared by hydrothermal method have comparable physical properties with the nanoparticles prepared using organic decomposition methods. Moreover, this method is environmentally friendly and easy to manage. Even in the spite of all benefits, the hydrothermal synthesis has not been extensively studied and used for the preparations of magnetic nanoparticles.

In this work, the preparation of nanoparticles by hydrothermal method and their characterizations by different physical methods are given. Influence of various parameters (annealing temperature, etc.) to the final properties of prepared nanoparticles is also studied. Cobalt chromite ($CoCr_2O_4$) has been chosen for its promising multiferroic properties.

Chapter 2

Theoretical part

2.1. Magnetic Properties

Magnetism, as a phenomenon, has to be seen from the point of view of quantum mechanics. The magnetic moment of free atoms has three principal sources[3]:

- Spin magnetic moment m_s, which originate from spin angular momentum of electron *S*
- Orbital magnetic moment m_l, which originate from orbital angular momentum of electron *L*
- Induced magnetic moment, which originate from the change of orbital momentum induced by external magnetic field

The first two effects give paramagnetic contribution to the magnetization while the third one gives diamagnetic contribution and it has an opposite direction to the external magnetic field as a result of the Lenz law. This effect occurs in all atoms, but it is observed only in the molecules or atoms with completely filled electron shells, which have the first two contributions equal to zero. In atoms with non-paired electrons, the paramagnetic contribution prevails over diamagnetic contribution, which is negligible.

The magnetization *M* is defined as magnetic moment of unit volume of the substance:

$$M = \frac{1}{V} \cdot \sum_{j} m_j \qquad (2.1)$$

where V represents the volume of the substance and m_j represents the magnetic moment of individual atoms. Electromagnetic field is described by Maxwell equations. The physical

units are represented by magnetic field strength, *H* (Ampere`s Law), and magnetic induction, *B* (Faraday Law). Their relation in vacuum can be expressed by the following equation[4]:

$$\vec{B} = \mu_0 \cdot \vec{H} \qquad (2.2)$$

where μ_0 stands for the permeability of vacuum and it is equal to $4\pi \times 10^{-7}$ kg·m·s^{-2}·A^{-2} (T/A). Magnetic state of the system (Sommerfeld system) is specified by the magnetization, *M*, which is related to *B* and *H* by the following expression:

$$\vec{B} = \mu_0 \cdot (\vec{H} + \vec{M}) \qquad \vec{M} = \chi \cdot \vec{H} \qquad (2.3)$$

where χ is magnetic susceptibility of a given material. For the substances with a negative magnetic susceptibility, the induced magnetic polarization has an opposite sign to the applied field. These substances are called diamagnetics. Substances with positive magnetic susceptibility are called paramagnetics. In the following chapters, the properties of magnetically ordered and disordered materials will be described. Some types of these magnetic structures are given in the Figure 2.1.

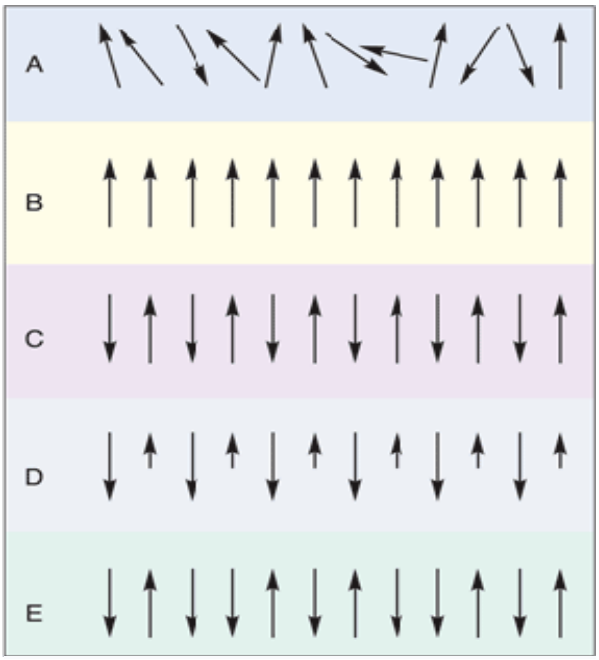

Figure 2.1. Some types of magnetism: A: paramagnetism, B: ferromagnetism, C: antiferromagnetism, D: ferrimagnetism and E: enforced ferromagnetism.

2.1.1. Substance without spontaneous magnetic ordering

2.1.1.1. Diamagnetism

Diamagnetism is characteristic for the substances that have only "non-magnetic" atoms and their magnetization, induced by the magnetic field, is very weak and it is opposite to the direction of applied magnetic field. The susceptibility, virtually independent on the applied magnetic field and temperature, is negative. There are two terms of the Hamiltonian, which contain the magnetic field[5]:

$$H_z = -\frac{\mu_B}{\hbar} \cdot (L_z + 2S_z) \cdot B_0 \tag{2.4}$$

$$H_{dia} = \frac{e^2 \cdot B_0^2}{8 \cdot m} \sum_{j=1}^{N_e} \left(x_j^2 + y_j^2\right) \tag{2.5}$$

where N_e is the number of electrons in the ion or the atom. The first term describes electron free motion and interaction of orbital momentum with magnetic field $B = \mu_0 \cdot H$, and the second term describes the diamagnetism.

Diamagnetic susceptibility can be expressed as the derivative of the magnetization M with respect to B_0 [6]:

$$\chi^{dia} = \mu_0 \left(\frac{\partial M}{\partial B_0}\right) = -\frac{N \cdot e^2 \cdot \mu_0}{6 \cdot m \cdot V} \sum_{j=1}^{N_e} \langle 0 | r_j^2 | 0 \rangle \tag{2.6}$$

The negative sign can be understood as the expression of the Lens law.

2.1.1.2. Paramagnetism

Paramagnetism corresponds to a positive magnetic susceptibility. Positive contribution to χ is found in[3]:

- Ions and free atoms with a partially filled electron shell
- Atoms, molecules and lattice defects having odd numbers of electrons where total spin of the system is not zero
- Metals (conduction electrons can also give rise the paramagnetic behaviour − Pauli paramagnetism)
- Rarely occurring compounds with even number of electron like molecular oxygen, organic biradicals

Paramagnetism means that an applied magnetic field induces a magnetization that is aligned parallelly with the applied magnetic field which caused it. The magnetic moment of an atom is associated with its total angular momentum:

$$\vec{J} = \vec{L} + \vec{S} \tag{2.7}$$

where $\vec{S}$ is spin moment and $\vec{L}$ is orbital moment. Magnetic moment of free atoms is given by the following equation[7]:

$$\mu = \gamma \cdot \hbar \cdot J = -g \cdot \mu_B \cdot J \tag{2.8}$$

where γ is the ratio of the magnetic moment to the angular moment and g is the g-factor. For the spin of electron, its value is g = 2.0023. For free atom, the g-factor is given by Landé equation:

$$g \approx 1 + \frac{J \cdot (J+1) - L \cdot (L+1) + S \cdot (S+1)}{2 \cdot J \cdot (J+1)} \tag{2.9}$$

The energy levels of atoms with non-zero magnetic moment interacting with external magnetic field can be expressed[3]:

$$E = -\vec{\mu} \cdot \vec{B} = -m_{\mathrm{J}} \cdot g \cdot \mu_{\mathrm{B}} \cdot B \tag{2.10}$$

where m_{J} is projection of total angular momentum, *J,* to the direction of magnetic field. Occupation of an energy level can be expressed using Boltzmann distribution:

$$\frac{N_i}{N} = \frac{exp^{-\frac{E_i}{k_{\mathrm{B}} \cdot T}}}{\sum_{\mathrm{j}} exp^{-\frac{E_j}{k_{\mathrm{B}} \cdot T}}} \tag{2.11}$$

and average magnetic moment of the atoms contributes to overall magnetic moment of the sample. For example, when we assume two-level system (where $J = 1/2$, $E = \pm \mu \cdot B$), the total magnetic moment of N atoms without spin-spin interaction, μ, in magnetic field, B, is[3]:

$$\mu_{\mathrm{N}} = \frac{N_{\uparrow} - N_{\downarrow}}{N_{\uparrow} + N_{\downarrow}} \cdot N \cdot \mu = \frac{e^{\frac{\mu \cdot B}{k_{\mathrm{B}} \cdot T}} - e^{-\frac{\mu \cdot B}{k_{\mathrm{B}} \cdot T}}}{e^{\frac{\mu \cdot B}{k_{\mathrm{B}} \cdot T}} + e^{-\frac{\mu \cdot B}{k_{\mathrm{B}} \cdot T}}} \cdot N \cdot \mu = N \cdot \mu \cdot \tan \frac{\mu \cdot B}{k_{\mathrm{B}} \cdot T} \approx \frac{N \cdot \mu^2 \cdot B}{k_{\mathrm{B}} \cdot T} \tag{2.12}$$

Atoms with higher magnetic moment have more energy levels, but the obtained result for the weak field approximation (Curie law) can be expressed as:

$$\chi = \frac{N}{V} \cdot \frac{J \cdot (J+1) \cdot g^2 \cdot \mu_{\mathrm{B}}^2}{3 \cdot k_{\mathrm{B}} \cdot T} = \frac{N}{V} \cdot \frac{p^2 \cdot \mu_{\mathrm{B}}^2}{3 \cdot k_{\mathrm{B}} \cdot T} = \frac{C}{T} \tag{2.13}$$

where p is an effective number of Bohr magnetons and C is Curie constant.

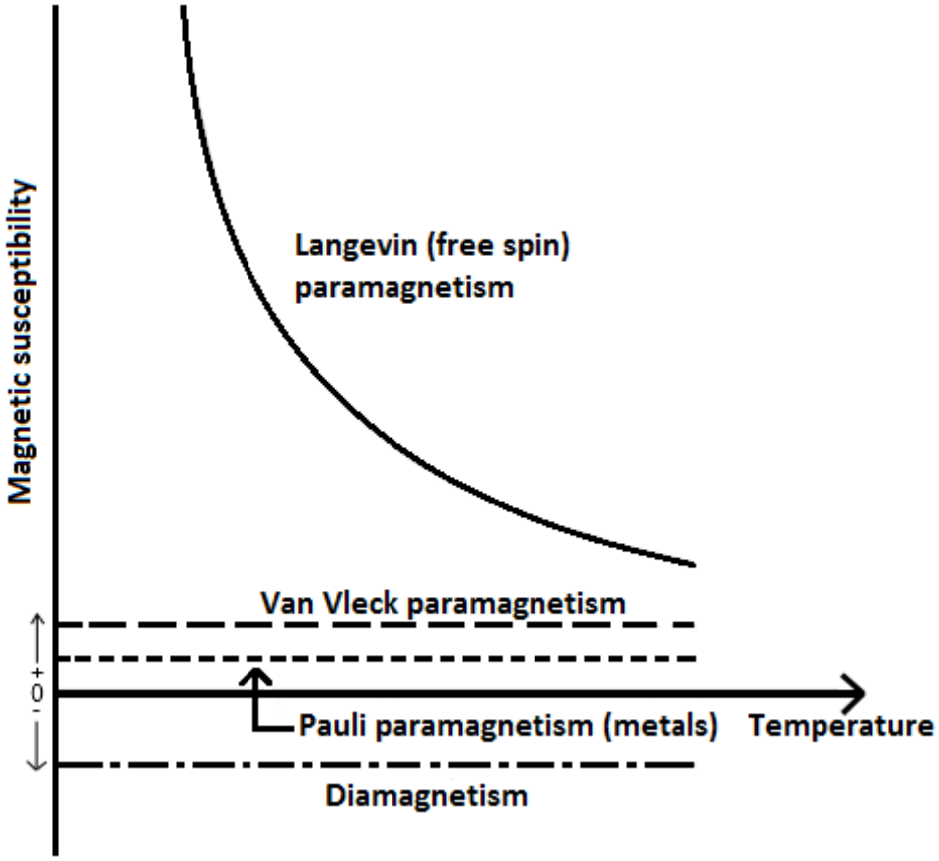

Figure 2.2. Characteristic curves of individual contribution to the susceptibility of paramagnetic system.

2.1.2. Spontaneous magnetism

Magnetic behaviour of bulk materials has its origin in the interactions of paramagnetic atoms or molecules. These interactions lead either to magnetically disordered or magnetically ordered materials, depending on how adjacent magnetic spins cooperate with each other. Although magnetic interactions occur in three dimensions, the type and strength of these interactions can vary in respective directions. This anisotropy can give rise to magnetic materials with one cooperative interaction type in one direction and different cooperative interaction types in the other two directions.

2.1.2.1. Ferromagnetism

Ferromagnetic materials have spontaneous magnetic moment, i.e. they can have non-zero magnetic moment, even in zero applied magnetic field (electron spins and magnetic moments

are regularly ordered). For ferromagnet in an applied field B, the respective Hamiltonian can be written as [5] :

$$\widehat{\mathcal{H}} = -\sum_{ij} J_{ij} \cdot S_i \cdot S_j + g\mu_B \sum_j S_j \cdot B \qquad (2.14)$$

where the first term represents the Heisenberg exchange energy and second term stands for the Zeeman energy. When the interactions between magnetic moments are sufficiently high, spontaneous ordering occurs below the Curie temperature T_c. It can be explained by the first term of this equation. For positive J, magnetic moments prefer parallel alignment, and this leads to ferromagnetic behaviour. For temperatures $T > T_c$, thermal motion overcomes spontaneous ordering, and the resulting behaviour is paramagnetic. It can be described by Curie-Weiss law [5]:

$$\chi = \frac{C}{T - T_c} \qquad (2.15)$$

Ferromagnetic materials have a spontaneous magnetization even in the absence of an applied field. Magnetic moments in these materials are arranged into domains. In each domain, there is an uniform arrangement of the magnetic moments, but the magnetization of each domain is directed in the different direction. This is caused by minimization of energy of magnetic field in surrounding free space. The borders between domains are called Bloch walls. Their thickness and size are given by anisotropy energy. Movement of Bloch walls and reorientation of moments can be forced by external magnetic field and then ferromagnetic material shows non-zero overall magnetic moment. The dependence of the magnetization on the magnetic field intensity is called hysteresis loop (Figure 2.3.).

The hysteresis loop has following important parameters:

- coercive field H_c corresponds to the magnetic field necessary to bring the overall magnetization, M, to zero

- remnant magnetization M_r corresponds to the magnetization showed by the sample after removing of the external applied field

- saturation magnetization M_s corresponds to a magnetization, when all magnetic moments are aligned with applied magnetic field and this magnetization does not increase with the further increasing of the applied magnetic field.

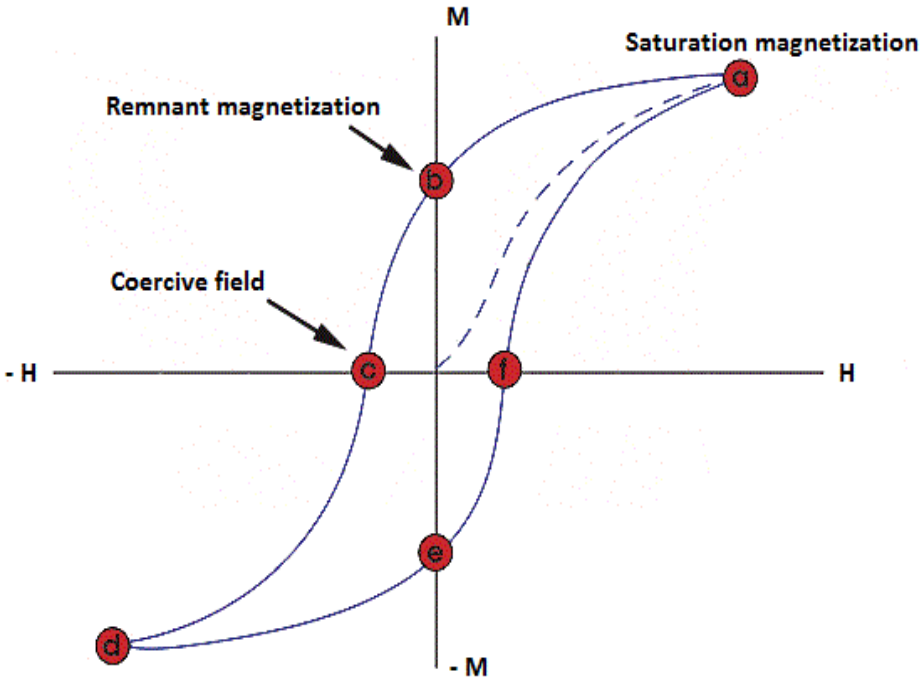

Figure 2.3. Hysteresis loop. Inner area of the curve is proportional to the density of energy, which is converted into heat during the full magnetization cycle.

When we decrease the size of the particles of ferromagnetic material we reach the critical size below it no Bloch walls can be formed and the particles contain only one domain (Figure 2.4.).

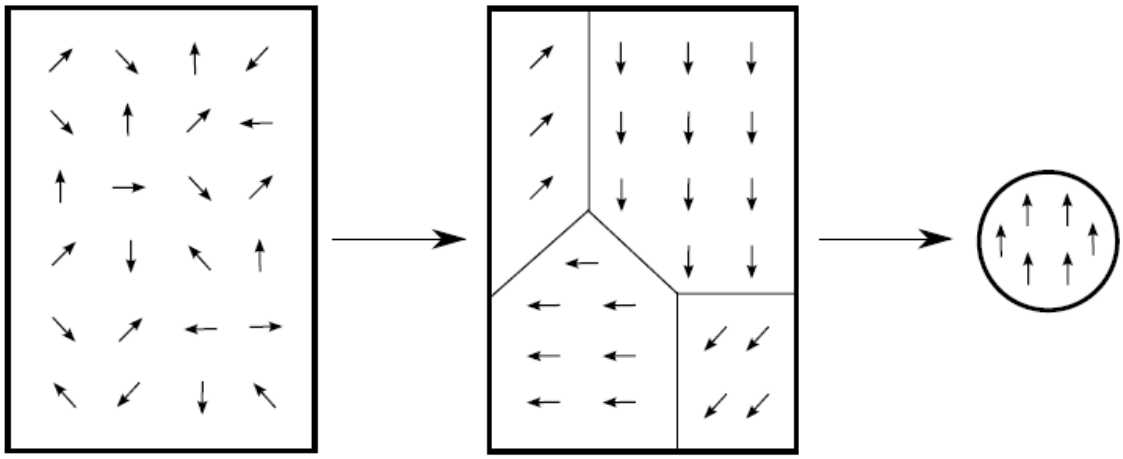

Figure 2.4. From left to right: paramagnetic material, multidomain ferromagnet and single domain particle.

2.1.2.2. Antiferromagnetisms

In the case of ferromagnetic behaviour, the interaction integral has positive sign and the vectors s_i and s_j are aligned parallel one to another in order to minimize the energy. For $J < 0$ the Hamiltonian [5]:

$$\mathcal{H} = 2 \cdot |J| \sum_{\langle i,j \rangle} s_i . s_j \tag{2.16}$$

gives rise to antiparallel alignment of the neighbouring spins. Materials with negative exchange integral ($J < 0$) have antiferromagnetic properties. The magnetic susceptibility of antiferromagnet increases as the temperature increases, up to the transition temperature, which is called Néel temperature:

$$T_N = \frac{|J|}{k_B} \tag{2.17}$$

The antiferromagnet is in the paramagnetic state above T_N. The magnetic susceptibility can be expressed by Curie-Weiss law[5]:

$$\chi \propto \frac{1}{T - \theta} \tag{2.18}$$

where θ is Weiss temperature. If $\theta = 0$ then the material is a paramagnet. If $\theta > 0$ the material is ferromagnet and $\theta = T_c$ and if $\theta < 0$ then the material is antiferromagnet and $\theta = -T_N$.

2.1.2.3. Ferrimagnetisms

In Figure 2.5. we can see two different sublattices in antiparallel arrangements. If these two sublattices have the different value of magnetic moment, then the overall magnetic moment is non-zero and we have a ferrimagnetic behaviour instead of an antiferromagnetic one. Thus ferrimagnetism can be considered as the special case of antiferromagnetism.

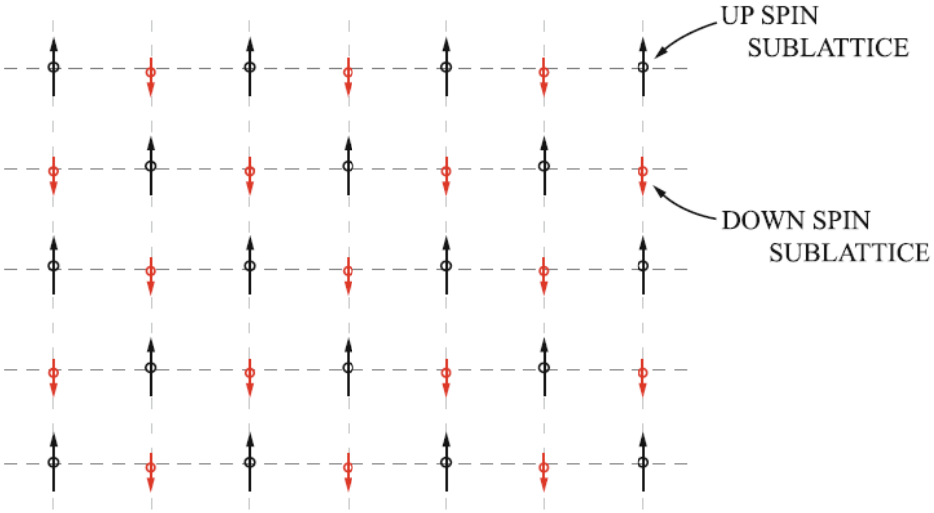

Figure 2.5. Sublattice structure of spins in a ferrimagnet.

2.1.3. Magnetism in nanoparticles

Nanoparticles represent the particles with the sizes ranging from 1 to 100 nm. Size effects constitute a fascinating aspect of nanomaterials. The smaller the particles are, the larger the surface area is, and this increase of the surface area leads not only to the increase of the material "reactivity" but also to the dramatic changes of magnetic properties.

2.1.3.1. Superparamagnetism

The magnetization of a small, single domain ferromagnetic particle is often constrained to lie parallelly or antiparallelly to the particular direction called the easy axis of magnetization. This phenomenon is due to the magnetocrystalline anisotropy or shape anisotropy. Let's have

the distribution of these small ferromagnetic particles in a diamagnetic matrix and let's assume that the particles are sufficiently distant one from another so that the interparticle interaction can be neglected. Monodomain particles with anisotropy energy K have a fixed direction of the magnetization in easy axis at low temperature (blocked state). The energy necessary for reorientation of magnetic moment of the whole particle is:

$$E_A = K \cdot V \cdot \sin^2 \theta \tag{2.19}$$

where θ is the angle between easy axis and magnetization, and V is volume of the particle.
For $k_B \cdot T >> K \cdot V$, the system will have paramagnetic-like behaviour. The atomic moments in the range of one nanoparticle are ordered and form one resulting moment, which is randomly oriented due to thermal agitation. The system of all nanoparticles then shows the superparamagnetic behaviour. The relaxation time τ of the magnetic moment of a particle is given by following equation[6]:

$$\tau = \tau_0 \cdot e^{\frac{K \cdot V}{k_B \cdot T}} \tag{2.20}$$

where τ_0 has typical value of about 10^{-9} s. Typical dependence of magnetization on temperature for nanoparticles, which are in superparamagnetic state, is shown on Figure 2.6. This figure represents a measurement of magnetization during zero-field-cooled (ZFC) and field-cooled (FC) mode. Sample is put into magnetometer and cooled under zero magnetic field down to 2 K, then a small magnetic field is applied and the magnetization of the sample is measured with increasing temperature of the sample (ZFC). For field-cooled measurement, the sample is cooled, with applied magnetic field. FC curve is recorded during the increase of the temperature. ZFC and FC curves come together at the temperature T_{B1} when all particles are in superparamagnetic state. ZFC curve shows the maximum at the temperature T_{B2} when the majority of particles are unblocked and are in superparamagnetic state.

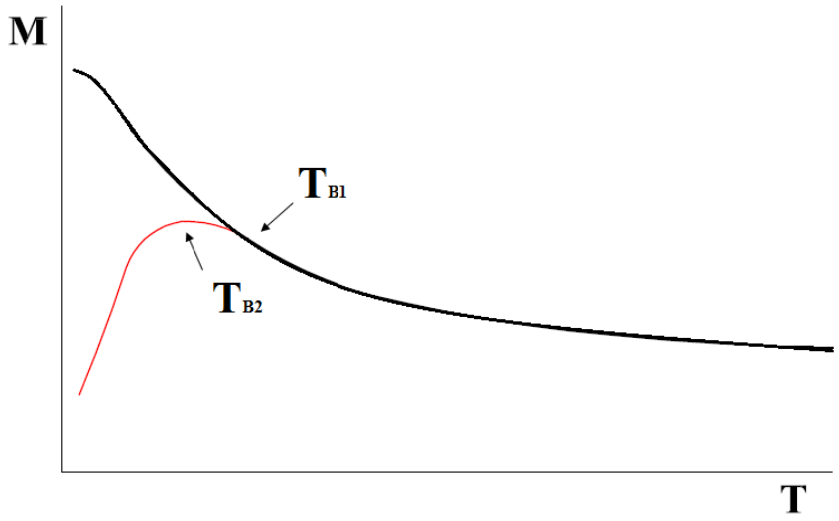

Figure 2.6. Temperature dependence magnetization.

2.1.3.2. Interparticle interactions

In magnetically diluted system, the pure superparamagnetism can occur. In these systems, the interparticle distances are too long and therefore the interparticle interactions can be neglected. In real system, the particles are relatively close to each other and, therefore, the interactions cannot be neglected and they must be taken into account when interpreting the magnetic properties. There are some different types of interactions:

- dipolar interactions - they are always present and they have anisotropic character.
- direct exchange interactions - for nanoparticles in ferro/antiferromagnetic matrix or for nanoparticles in a close contact.
- superexchange interactions - for metal nanoparticles in a metal matrix.
- RKKY interactions - for particles in insulating matrix.

It is difficult to determine experimentally, which interaction plays the decisive role in the sample, because the different effects produced by interactions, like particle shape, size distribution and surface effects, are superposed and they influence the magnetic properties. The systems can be classified according to the strength of interparticle interactions.

A. Weakly interacting systems:

A.1. Superparamagnet with interactions

Dipolar interactions are considered as a disturbance of superparamagnetic state. The interactions have an influence on the blocking temperature. This phenomenon results in the saturation of temperature dependence magnetization curves below the blocking temperature (FC curves).

A.2. Superferromagnet (SFM)

The existence of dipolar interaction gives rise to the ferromagnetic coupling between spins, which does not affect the position of blocking temperature. The temperature dependence of susceptibility above the blocking temperature obeys Curie-Weiss law and under blocking temperature again leads to saturation of FC curves.

B. Strongly interacting systems

B.1. Superspin glass (SSG)

It can be described as a randomly interacting magnetic system characterized by randomly synergistic freezing super-spins at a defined temperature of freezing (furcation), T_f. At the temperature above the T_f, the individual super-spins (magnetic moments of individual particles) are independent, and system is in the superparamagnetic state. The effects of dipolar interactions at lower temperature than T_f causes that the nanoparticles form the local correlated units (clusters) and the system is therefore in a metastable state without long range magnetic ordering and it has slow relaxation. It results in the dynamic behaviour of the system which depends on the history of the system. This phenomenon is called "memory effect".

B.2. Superspin glass-like system (SSG-like system)

This system has the attributes like superspin glass but the behaviour of nanoparticles is different, this system does not have a "memory effect".

2.2. Characterization Method

2.2.1. Electron Microscopy (EM)

Electron microscopy is used for morphological studies of submicron structures with higher magnification and resolution. Electron microscopes use the electron as a particle, which carries information about structure of matter. Due to wave-corpuscular character of electron, it is possible to ascribe a wavelength to the electron using de Broglie equation. Absolute wave function of the free electron is:

$$\psi(\vec{r}, t) = e^{i\cdot(\vec{k}\cdot\vec{r}-\omega\cdot t)} \tag{2.21}$$

when ψ is wave function, r is position vector, k is wave vector, ω is angular frequency and t is time. There are two main types of electron microscope: transmission electron microscope (TEM) and scanning electron microscope (SEM). The optics of the TEM is similar to the conventional transmission light microscope, while the SEM resembles more likely the scanning confocal laser microscopes.

2.2.1.1. Transmission Electron Microscopy (TEM)

The differences between light microscope and TEM consist in the fact that the visible light beam is replaced by an electron beam and glass lenses are replaced by electromagnetic ones. The construction of a transmission electron microscope and the optical path is showed in the Figure 2.7. It is a technique where a beam of electrons is transmitted through an ultra thin specimen and it interacts with this specimen during the passage through it. The crystalline sample interacts with the electron beam mainly by diffraction rather than absorption. The intensity of the diffraction depends on the orientation of the planes of atoms in crystal relative to the electron beam. There are two mechanisms by which electron scattering forms images: mass-density contrast and diffraction contrast.

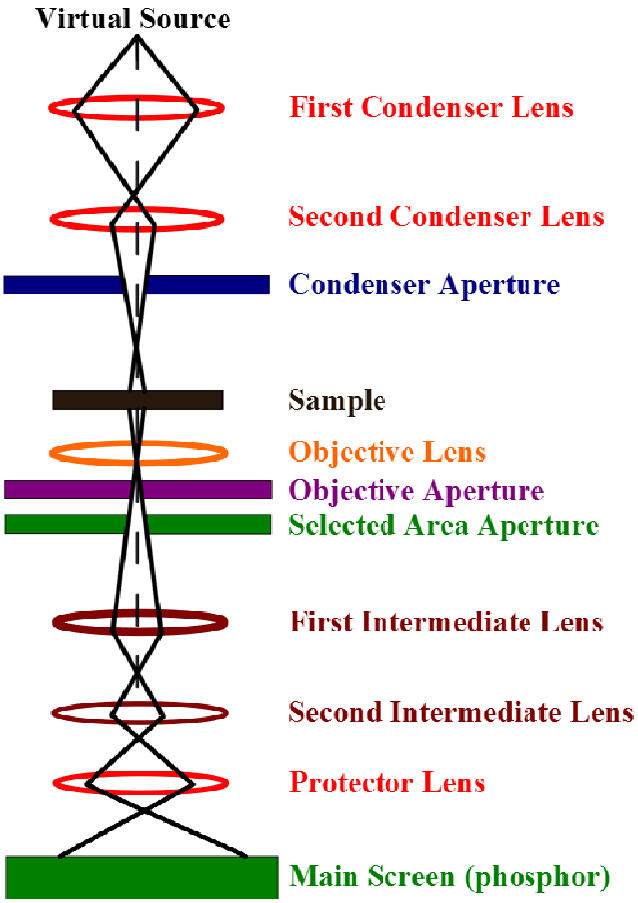

Figure 2.7. Scheme of the optical path of transmission electron microscope.

2.2.1.2. Scanning Electron Microscopy (SEM)

In this electron microscope, the images are formed by the scanning of the sample surface with a high energy beam of electrons. The main difference between SEM and TEM is that the electrons from the sample in the SEM are "reflected" and do not pass through the sample (with the exception of STEM - scanning transmission electron microscopy). The electron beam interacts with the specimen and gives the signal in the form of secondary electrons or back scattered electrons. Moreover, the characteristic X-rays radiation is generated. It bears information about the elements composition of the sample and about the topography of the elements on the surface. Secondary electrons (SE) are used for displaying the morphology of the sample. X-rays are used to identify the elemental composition of the sample (EDX). Backscattered electrons (BSE) images are often used in analytical SEM along with the spectra obtained from the characteristic X-ray radiation. Electron microscope consists of electron gun, electromagnetic lenses, screen, scanning lens, detector for secondary and scattered electrons, and sample holder.

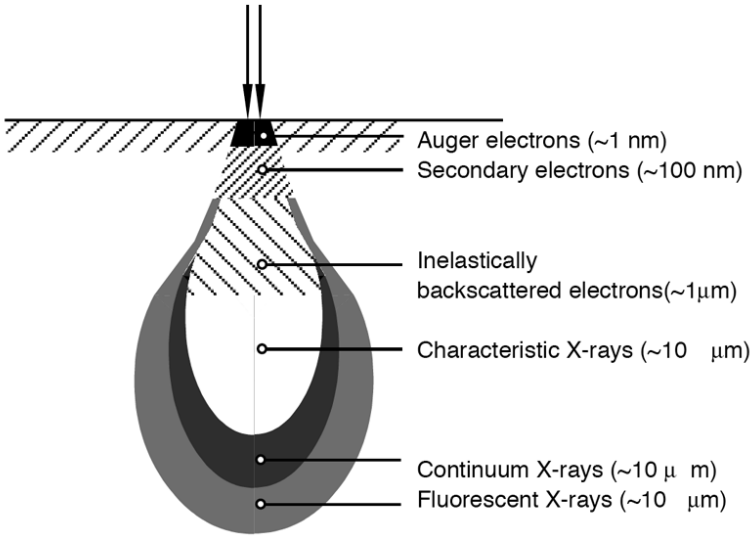

Figure 2.8. Electron beam interacting with the sample. The depth of output of the individual species of radiation is given in the brackets.

2.2.1.3. Energy Dispersive X-ray Analysis (EDX)

Energy dispersive X-ray analysis is a technique for the analysis of the elements near the surface and for determination of their content. It is also possible to obtain the overall mapping of the sample. Using EDX, the composition of the nanoparticles can be determined in the sample (entire volume), providing that they contain some heavy metals ions. This method is not so well adapted for the determination of the elements with low atomic number.

2.2.1.4. High Resolution Transmission Electron Microscopy (HRTEM)

High resolution transmission electron microscopy is an imaging mode of the transmission electron microscope that allows the imaging of the crystallographic structure of a sample at the atomic scale. The contrast arises from the interference in the image plane of the electron wave with itself. Each imaging electron interacts independently with the sample and these interactions result in a wave passing through the imaging system of the microscope. The resulting image then shows the fringes which correspond to the interlayer distances of direct crystal lattice.

2.2.2. Powder X-ray Diffraction (PXRD)

It is the most important technique used for phase identification of a crystalline material and it gives information about unit cell dimensions. X-ray diffraction is based on constructive interference of monochromatic X-rays and crystalline samples. X-ray radiation is generated by a cathode radiation tube. The interaction of X-ray radiation with sample gives rise to the secondary "diffracted" X-ray beam whose direction depends on the interplanar distances in the crystalline structure according to Bragg`s Law:

$$n \cdot \lambda = 2 \cdot d \cdot \sin\theta \tag{2.22}$$

where n is an integer, λ stands for the wavelength of the X -rays, θ is the diffraction angle and d is the interplanar distances.

In the case of nanocrystalline materials, the crystallite size can be calculated from the width of the peaks using Scherer equation:

$$d = \frac{K \cdot \lambda}{B \cdot \cos\theta} \tag{2.23}$$

where K is Scherrer`s constant, λ is wavelength of the used x-ray radiation, B is width of diffracted peak (in angle θ).

2.3. Spinel Structure

The general formula of spinel structure can be written as $A^{2+}B_2^{3+}O_4^{2-}$. Materials with this structure have interesting magnetic, optical and electric properties. The cubic spinel structure is characterized by space group of $Fd\bar{3}m$. Unit cell contains 8 formula units of AB_2O_4 (Figure 2.9.). In the normal spinel structure, there are 8 atoms of metal (A) placed in the tetrahedral sites and 16 atoms of metal [B] occupy the octahedral sites. There can be also an inverse spinel structure, in which half of the cations [B] occupy tetrahedral positions, while the second half of the B cations and A cations occupy the octahedral positions. The formula can be written as $(B)_t[AB]_oO_4$, where parentheses stand for the tetrahedral sites and square brackets stand for octahedral sites. The occupation of the octahedral positions may be random or ordered. Distribution of cations depends on several parameters:

- the electron configuration
- the method of preparation
- the relative size of the cations and anions and their diameter
- the electrostatic energy
- the conditions of synthesis

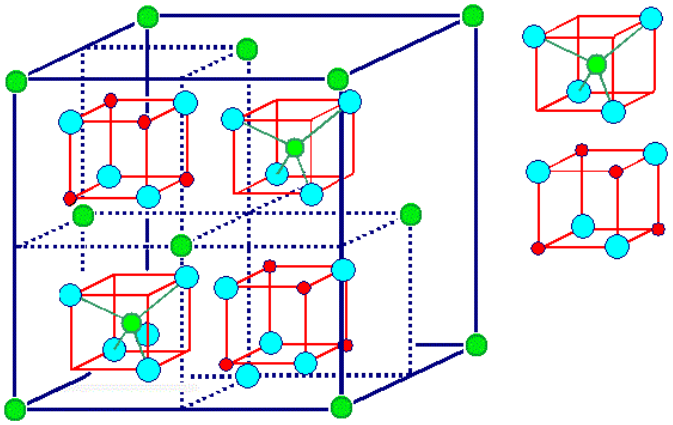

Figure 2.9. Spinel structure (AB_2O_4), where blue spheres stand for oxygen, green spheres for the cations in tetrahedral sites and red spheres for cations in octahedral sites. The red cubes are located at the back part of the unit cell.

2.4. Cobalt Chromite - Structure and Magnetic Properties

Up to date, the studies of magnetic nanomaterials were focused mostly on spinel ferrites and there are few works concerning the chromite nanoparticles. Moreover, the chromites are considered to be promising multiferroic materials.

$CoCr_2O_4$ has a spinel structure, with Co^{2+} and Cr^{3+} located in the centres of tetrahedra and octahedra respectively (Figure 2.10.). In the spinel oxide of $CoCr_2O_4$, which exhibits net magnetization, the multiferroicity has been observed[8]. $CoCr_2O_4$ is the first example of a multiferroic compound with both spontaneous magnetization and a polarization of spin origin. The direction of the spontaneous polarization, the spin-spiral axis, and the propagation vector are perpendicular to each other in accord with the spin-current model for magnetic ferroelectricity proposed by Katsura *et al* (Figure 2.11.)[9]. $CoCr_2O_4$, the cubic normal spinel ferrimagnet, has recently attracted much attention as a multiferroic material. The magnetic moment is composed of the ferrimagnetic component and the spiral component[10,11]. Spiral clusters in $CoCr_2O_4$ are characterized by their size distribution and their time scale. The distribution suggests a complex structure of the solution of the spin Hamiltonian. The spiral clusters might also change their properties under electric field, because the field separates the Co and Cr ions and the O ions in opposite directions, and breaks the subtle balance of the competition of the exchange interaction[12].

Different methods were used for the cobalt chromite preparation. One of the first preparations of cobalt chromite nanoparticles was carried out by Dutta etal.[13]. They report the synthesis of nanocrystalline $CoCr_2O_4$ by a fast sonochemical route, which is based on acoustic cavitations in a liquid. This method had several advantages, it is seedless, surfactant free, and template free. Rath etal. prepared the $CoCr_2O_4$ nanoparticles using coprecipitation method. They observed the transition from paramagnetic to superparamagnetic state[14,15]. Edrissi etal. improved the preparation method using organic precursors. They used mixed Cr^{3+} and Co^{2+} chelates of 2-mercaptopyridin N-oxide for the preparation of cobalt chromite NPs. The final product was found to have good catalytic properties for the oxidation of trichlorethylene[16]. Durani etal. prepared the cobalt chromites particles by hydrothermal synthesis. Their synthesis was carried on at higher values of pH (>10) and this procedure led to relatively bigger particle sizes (>100 nm)[17].

Deep study of magnetic properties and their interpretation was given by Chang etal.[18]. They described magnetic ordering of a spiral spin component with an incommensurate propagation vector that was observed at 26 K, while at 14.5 K, they observed the incommensurate conical spin order [18].

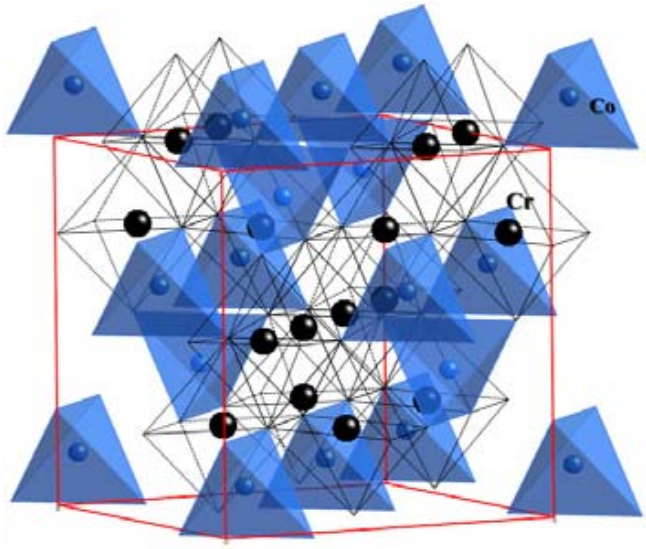

Figure 2.10. Crystal structure of $CoCr_2O_4$, where the Cr^{3+} cations (black) occupy open octahedral sites, the Co^{2+} (blue) occupy tetrahedral sites and the red line represents the unit cell [18].

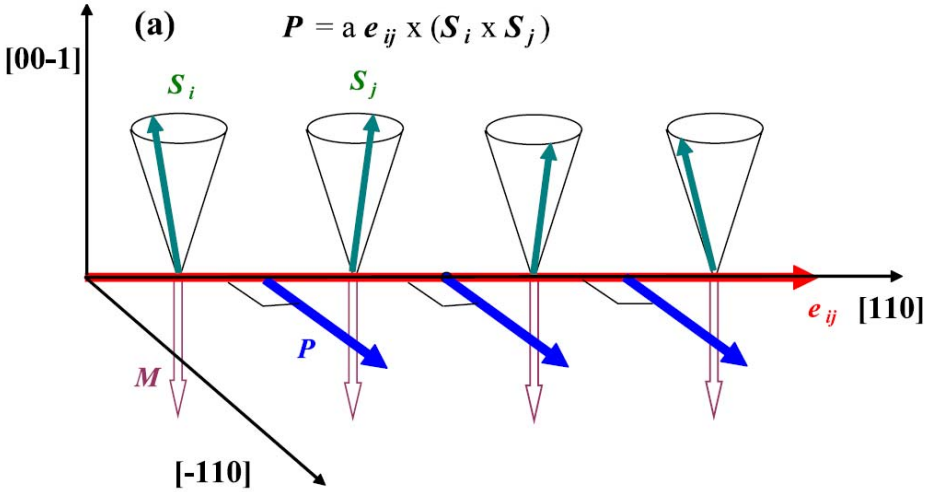

Figure 2.11. The spin-current model for the magnetic ferroelectricity proposed by Katsura *et al*[9]. where P is induced polarization, S_i and S_j are the canting spins, e_{ij} is vector connecting the two sites and a is the constant, which represent the spin exchange interaction and the spin-orbital interaction.

2.5. Hydrothermal Method

This method was used by Wang et al[2] for the preparation of NPs. It is a quite general synthesis and can be used for the preparation of various nanocrystals: metals (Ag, Pt, Au, Ru, Rh), magnetic (MFe_2O_4, M represents Fe, Co, Zn, Mg or Mn), dielectric ($MTiO_3$, M represents Ba, Sr), fluorescent (doped LaF_3, $NaYF_4$), semiconductors (CdSe, ZnSe, PbS). Hydrothermal method for nanoparticle preparation involves the treatment of the mixture of metal salt, fatty acid, its salts, ethanol and water in autoclave tube at increased temperature (up to 200 °C). Three phases are formed in the system: sodium salt of fatty acid (solid), the liquid phase is formed by ethanol and fatty acid (liquid), and water-ethanol solution containing metal ions (solution). A transport of the metal ions occurred spontaneously through the interface of solid and solution based on exchange of ions, which leads to the formation of metal salt of fatty acid and sodium ions enter into the aqueous phase. Then at the relevant temperature, the ethanol reduces the metal ions at the liquid-solid or solution-solid interfaces. This process is shown in Figure 2.12. Prepared NPs are capped with fatty acid and they are hydrophobic.

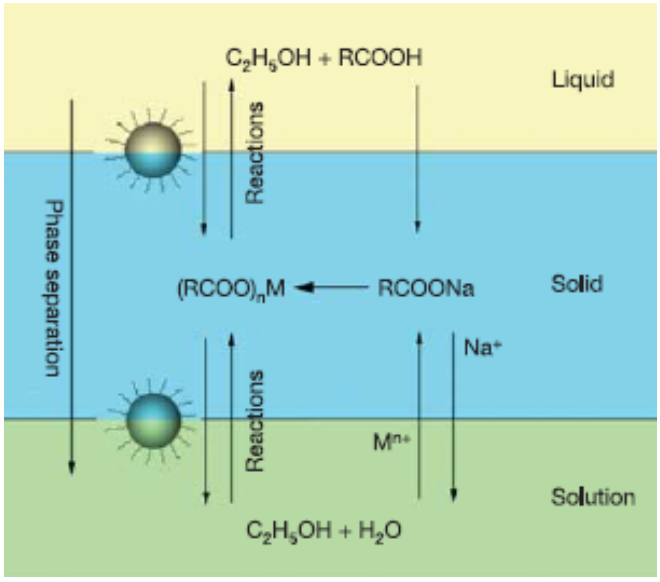

Figure 2.12. Scheme of the liquid-solid-solution (LSS) phase transfer[2].

Chapter 3

Experimental part

This part is focused on the preparation of isolated magnetic nanoparticles of cobalt chromite and their characterizations.

3.1. Characterization Methods

- Powder X-ray diffraction was carried out using PANalytical X`Pert PRO diffractometer with Cu K_α radiation equipped by secondary monochromator and PIXcel detector at Faculty of Science, Charles University, Prague. Step was 0.02°. Samples were dried into powder form and put on glass plate. Profile analysis in order to obtain particle size was done by FullProf WinPLOTR.

- Transmission electron microscopy was carried out using JEOL 200 at University of Cagliari in Italy. Samples were deposited on copper grid.

- High resolution transmission microscopy images were obtained with a JEM 2010 UHR equipped with a Gatan Imaging Filter (GIF) and a 794 slow scan CCD camera at University of Cagliari in Italy.

- Scanning electron microscopy measurements were obtained with Tescan Mira I LMH with energy dispersed X-ray detector (EDX) Bruker AXS at Faculty of Mathematics and Physics Charles University in Prague. Samples were deposited on carbon film.

- Thermogravimetry was carried out using STA 449 F1 Jupiter at J. Heyrovsky Institute of Physical Chemistry in Prague. Samples were heated up to 600 °C (heating rate 10 °C/min) in argon atmosphere.

- Magnetic measurement: zero-field-cooled (ZFC) and field-cooled (FC) magnetizations (applied field 5 mT) and hysteresis loops at various temperatures were measured on Quantum Design MPMS7XL and PPMS9 device (SQUID) at Joint laboratory for Magnetic Studies in Trója, Prague.

- Fourier transform infrared spectroscopy (FTIR) and Raman Spectroscopy was done at Faculty of Sciences of Charles University in Prague. FTIR spectra were obtained using Thermo Scientific Nicolet 6700 FTIR Spectrometer (resolution 2 cm^{-1}, DTGS detector, KBr beam splitter, Happ-Ganzel apodization, KBr windows, zero filling) in region 400 - 4000 cm^{-1} with nujol technique. Far infrared spectra were measured in the region of 400 - 50 cm^{-1} (resolution 4 cm^{-1}, Solid substrate TM beam splitter, DTGS detector, Happ-Ganzel apodization, PE window). Raman Spectroscopy was measured with Thermo Scientific DXR Raman Microscope with Olympus microscope in the spectral region of 50 - 1900 cm^{-1} with the resolution of 3 cm^{-1}. He-Ne or laser diodes (532 or 780 nm) were used. Spectrometer was calibrated by the calibration software using multiple neon emission lines and multiple polystyrene Raman bands and standardized with white light.

3.2. Chemicals

ethanol absolute	Penta-chemicals, p.a
1-pentanol	Aldrich, 99+%
hexane	Lach-ner
oleic acid	Aldrich, tech. 90%
sodium hydroxide	Lach-ner, p.a., micropearls
cobalt (II) chloride hexahydrate	Penta-chemicals, p.a
chromium (III) chloride hexahydrate	Aldrich, ≥98%

3.3. Synthesis of Nanoparticles $CoCr_2O_4$

The samples were prepared by hydrothermal method in autoclave (Berghof) with 50 ml teflon liner. Following amounts of reactants were used for the preparation: 10 mmol (400 mg) of sodium hydroxide, 12 mmol (3,39 g) of oleic acid, metal chlorides (Cr^{3+} : Co^{2+} = 2 mmol : 1 mmol). The preparation was carried out in the mixture of 15 ml of alcohol (ethanol/1-pentanol) and 20 ml of water. First, sodium hydroxide was dissolved in a small amount of water and then ethanol was added. This solution was directly mixed with oleic acid in order to avoid the formation of soap (clear solution was formed). Then the water solution of metal salts which serve as a precursor was added, and the reaction mixture became sticky. Then, the solution was sonicated for 5 minutes. Two phases were formed: water and organic phase. This reaction mixture was put into teflon liner (volume 50 ml), enclosed in the autoclave and placed into oven for 10 to 16 hours at the temperature of 200 °C.

After cooling of the autoclave, the following phases were obtained: upper oleic phase, which contained a small amount of nanoparticles, aqueous phase and sedimented nanoparticles. Liquid phase were discarded and remaining particles were dispersed in 15 ml of hexane. Then, the non-dispersed particles (aggregates) were separated using centrifugation and the hexane dispersion was used for the following preparation. Then, the nanoparticles were precipitated from dispersion using 10 ml of ethanol and separated by centrifugation (4500 rpm for 5 minutes). This procedure (dissolving in hexane, precipitation using ethanol) was repeated three times. The samples showing amorphous phase were heat treated at the furnace at various temperature. Final samples were characterized by instrumental methods.

After washing procedure of the samples, they were annealed at various temperatures from 300 °C to 500 °C (heating rate 1 °C/min).

This preparation scheme was applied to the samples, which are listed in the following Table 3.1.

Sample	Reaction composition				Reaction conditions		Annealing Temperature (°C)
	Ratio (Cr:Co)	**Alcohol** (ml)	**Water** (ml)	**Oleic acid** (ml)	**Reaction Temperature** (°C)	**Reaction Time** (h)	
DZ 300	2:1	E: 10	10	3.82	200	16	300
DZ 350	2:1	E: 20	20	3.82	200	16	350
DZ 400	2:1	P: 5	10	3.82	200	10	400
DZ 450	4:2	E: 10	15	6.37	200	16	450

Table 3.1. List of prepared samples and their parameters of preparation.

Chapter 4

Results and discussion

4.1. Discussion of Hydrothermal Synthesis

4.1.1. Oleic acid and sodium oleate system

In hydrothermal synthesis, oleic acid and sodium oleate serve as capping agents for the nanoparticles. These agents can be dissolved in some solvent, which could also dissolve other reactants. Sodium oleate was prepared directly from oleic acid and sodium hydroxide:

$$C_{18}H_{33}COOH + NaOH \rightarrow C_{18}H_{33}COONa + H_2O$$

Due to the fact that the water solution of NaOH reacts with oleic acid to form insoluble oleate, the mixture of water and ethanol was used. First, NaOH was dissolved in small amount of water and then ethanol was added. This solution can be mixed with oleic acid to give a clear solution. Minimal amount of water was found to be 1 ml for 0.4 g (10 mmol) of NaOH.

4.1.2. Metal oleate formation

After adding the water-ethanol solution of reactant precursor (cobalt and chromium chloride) to oleic acid-sodium oleate system, the reaction mixture becomes dark. Two-phase system, water phase and organic phase (containing metal oleates and remaining oleic acid), are formed after sonication.

$$3\ C_{18}H_{33}COONa + CrCl_3 \rightarrow Cr(C_{18}H_{33}COO)_3 + 3\ NaCl$$

$$2\ C_{18}H_{33}COONa + CoCl_2 \rightarrow Co(C_{18}H_{33}COO)_2 + 2\ NaCl$$

4.1.3. Particles formation

The process of particles formation is shown in Figure 4.1. The metal salts are hydrolyzed and precipitated into the water phase after reaching critical diameter.

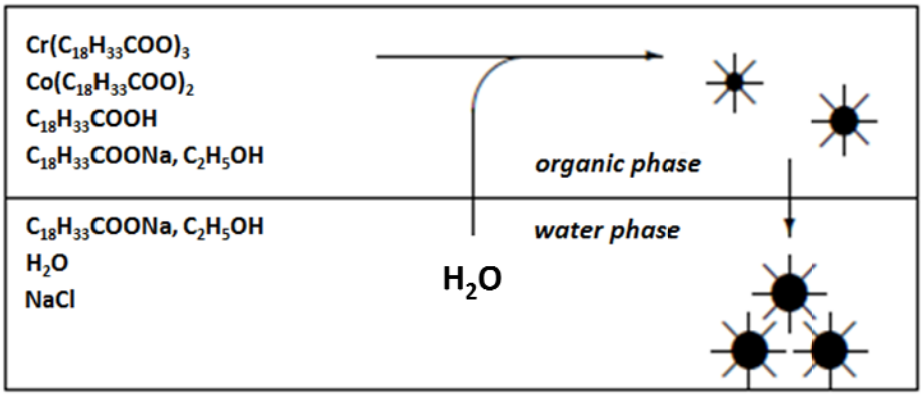

Figure 4.1. The scheme of the particles formation.

4.2. Powder X-ray Diffraction

The phase composition, particles size and lattice parameters of the prepared samples were determined by PXRD. The profile analysis was carried out by program FullProf and PANalytical X´pert High Score software. Measured diffraction patterns of the samples are shown in Figure 4.2. Two samples (DZ 300 and DZ 450) contained pure spinel phase only and the DZ 350, DZ 400 samples showed also a small amount of NaCl probably due to non sufficient washing procedure after hydrothermal reaction, but this fact has no negative impact on physical properties. Moreover, the DZ 350 sample contained also a small amount of Cr_2O_3.

The measured diffraction patterns were processed by Rietveld analysis using the program package FullProf [19]. The structure was specified by fitting of the structural model using measured data. The values of lattice parameter for each samples were determined. Using instrumental function, the real nanoparticles sizes were obtained. The experimental data and fits are shown in Figures 4.3 - 4.6. The position of measured maxima of each samples are consistent with the position of Bragg reflexion of the $CoCr_2O_4$ spinel structure. The values of NPs size and lattice parameter, which was obtained from fitting of the individual samples by Rietveld analysis, are shown in Table 4.3. It was found that the lattice parameters depend on annealing temperature. It can be explained by defects present in crystal lattice (dislocation, vacancies) and by small nanoparticles size. There are dangling bonds on the surface of nanoparticles and the crystal lattice is disordered. With the decreasing nanoparticle size the disorder increases, and it disappears with increasing temperature and increasing naparticles size. The tabulated value of lattice parameter of $CoCr_2O_4$ is 8.3299 Å (JCPDF 22-1084). In the prepared samples, the lattice parameter increases with the increasing annealing temperature. The best agreement of the lattice parameters with standard one (JCPDF 22-1084) was found for the sample DZ 450 heat treated at 450 °C.

It was found that the particles size depends on the annealing temperature. From Table 4.3., it can be seen that full width at half maximum (FWHM) gradually decreases corresponding to (spinel phase) particles growth with the increasing annealing temperature.

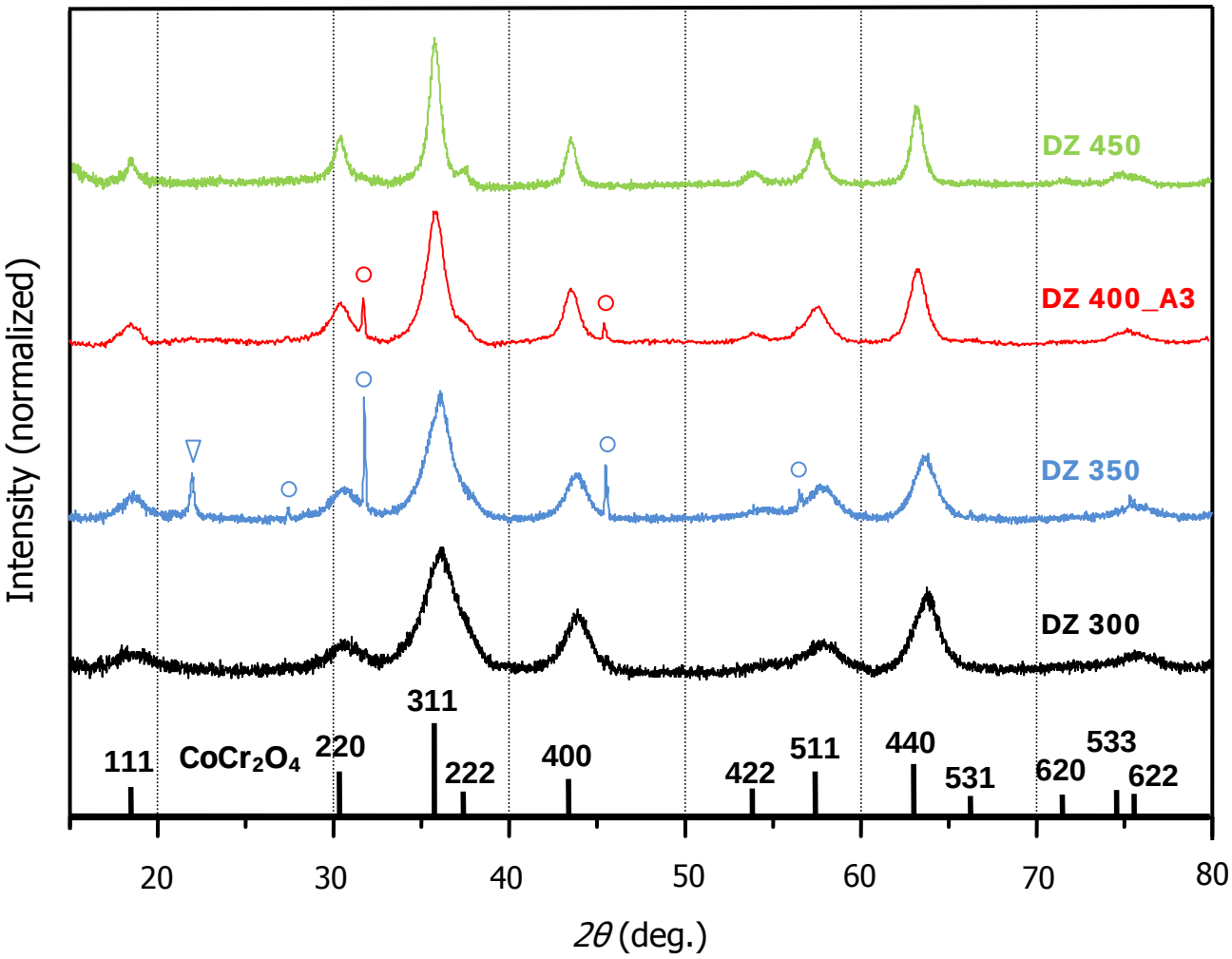

Figure 4.2. PXRD patterns of the samples. The vertical black lines correspond to the tabulated diffraction position of cobalt chromite ($CoCr_2O_4$). The DZ 300, DZ 450 contain only spinel phase. Other diffractions correspond to: ○ halite (NaCl), ▽ Cr_2O_3.

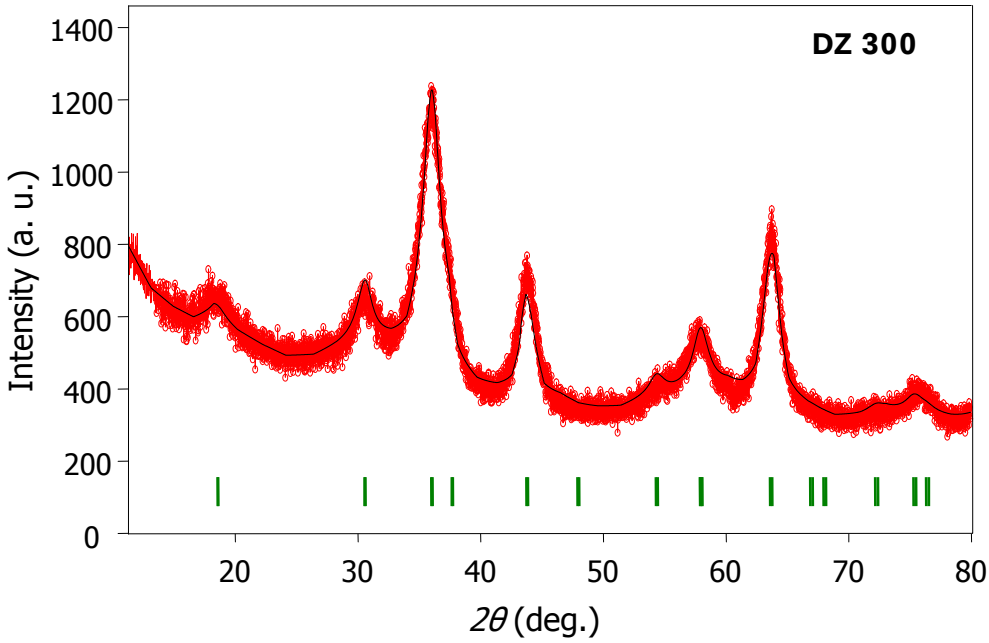

Figure 4.3. Experimental data of the PXRD of DZ 300 sample measurements and fitting using Rietveld method by program FullProf. The vertical lines (green) correspond to the position of Bragg maxima of $CoCr_2O_4$. The black line represents the fitting curve.

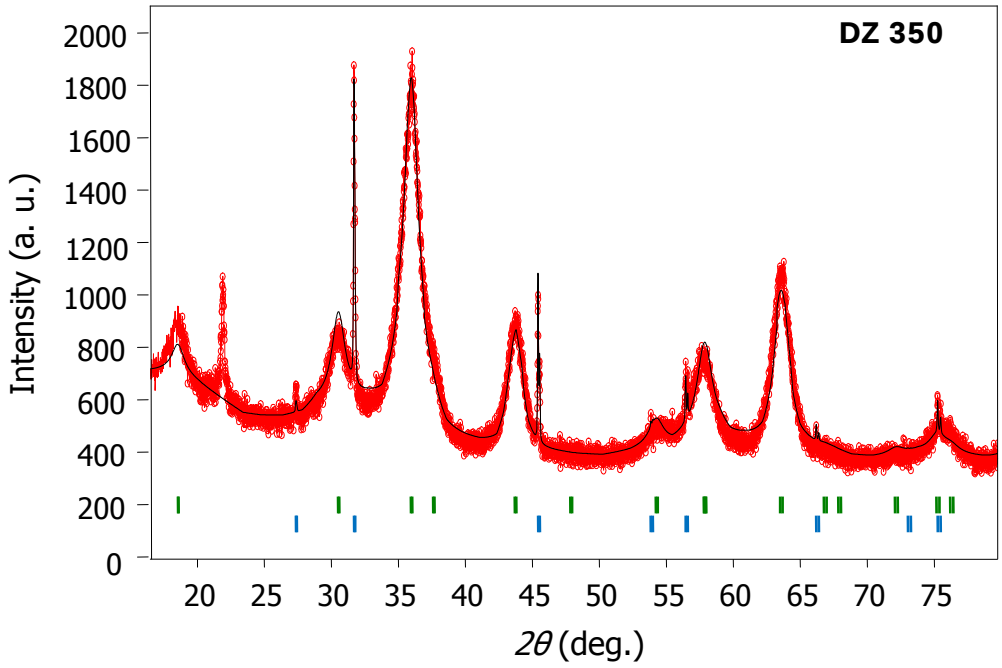

Figure 4.4. Experimental data of the PXRD of DZ 350 sample measurements and fitting using Rietveld method by program FullProf. The green vertical lines correspond to the position of Bragg maxima of $CoCr_2O_4$ and the blue to the position of Bragg maxima of NaCl. The black line represents the fitting curve.

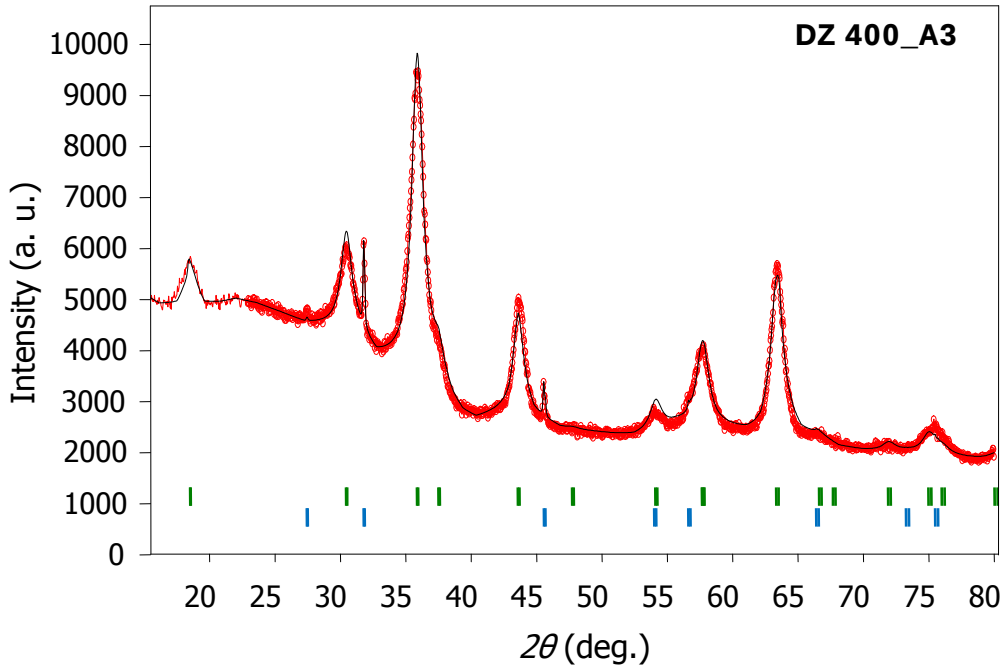

Figure 4.5. Experimental data of the PXRD of DZ 400_A3 sample measurements and fitting using Rietveld method by program FullProf. The green vertical lines correspond to the position of Bragg maxima of $CoCr_2O_4$ and the blue to the position of Bragg maxima of NaCl. The black line represents the fitting curve.

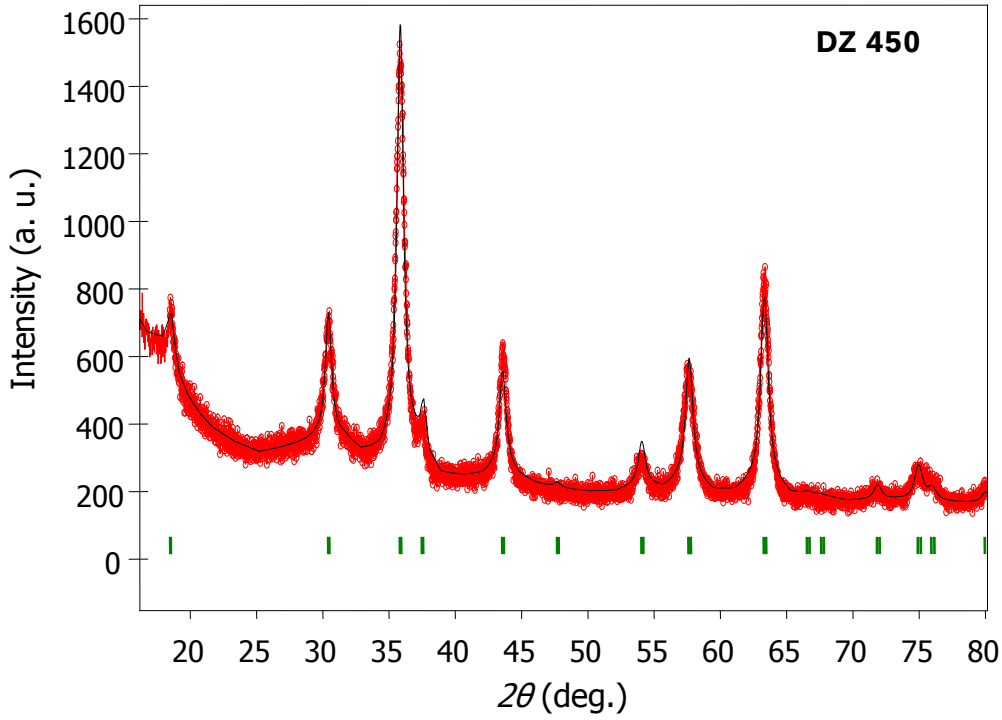

Figure 4.6. Experimental data of the PXRD of DZ 450 sample measurements and fitting using Rietveld method by program FullProf. The vertical lines (green) correspond to the position of Bragg maxima of $CoCr_2O_4$. The black line represents the fitting curve.

4.3. Electron Microscopy

4.3.1. TEM observations

The TEM observations were made in two different modes: bright field and dark field. The bright field mode gives us an information mainly about morphology of the samples. The dark field mode provides us an additional information about crystallinity of displayed nanostructures. From the following images, we can see that the samples consist of nanocrystals of the size of about 3 - 16 nm. Small white spots in the dark field mode images correspond to the crystalline part of particles with ordered crystal structure having suitable orientation with regard to the electron beam. The images of TEM observations were analyzed in order to obtain the information about particle size and its distribution. The size distribution histograms were obtained from the TEM images in order to correlate the physical properties of nanoparticles with the corresponding particles sizes and size distribution. The Figures 4.7. and 4.8. show the TEM images of the samples and corresponding calculated size distributions from the set of about 100 nanoparticles. As expected, the particles size increases with the increasing heat treatment temperature. The samples have also tendency to form aggregates.

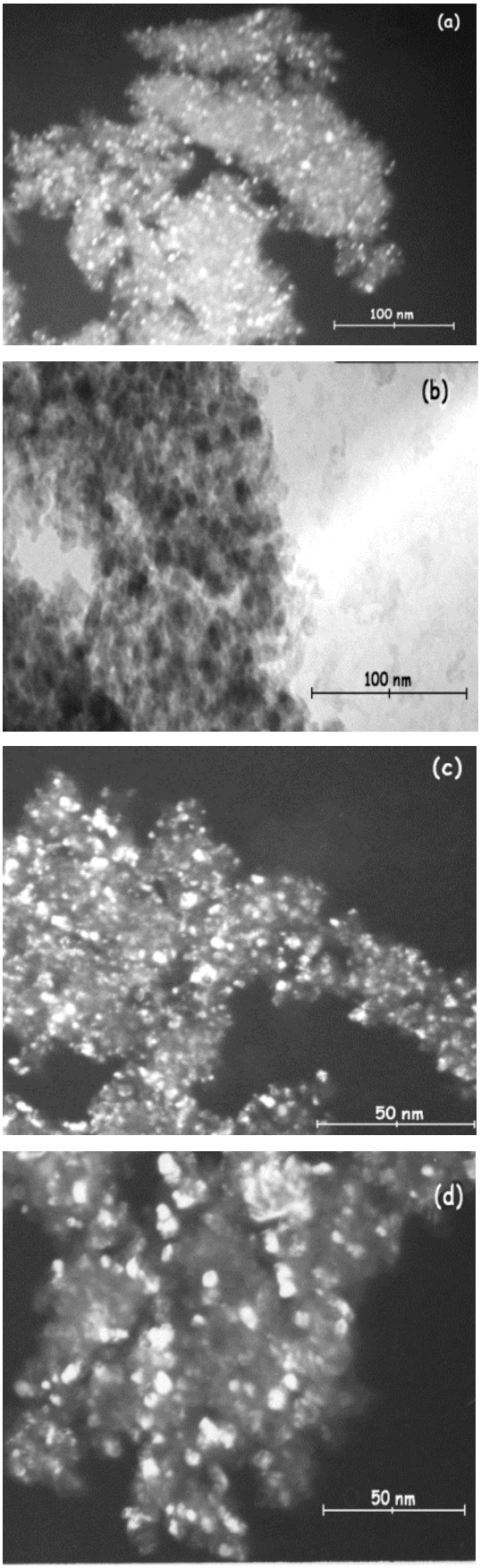

Figure 4.7. TEM images of the samples: a) DZ 300 (dark field mode) b) DZ 350 (bright field mode) c) DZ 400_A3 (dark field mode), d) DZ 450 (dark field mode)

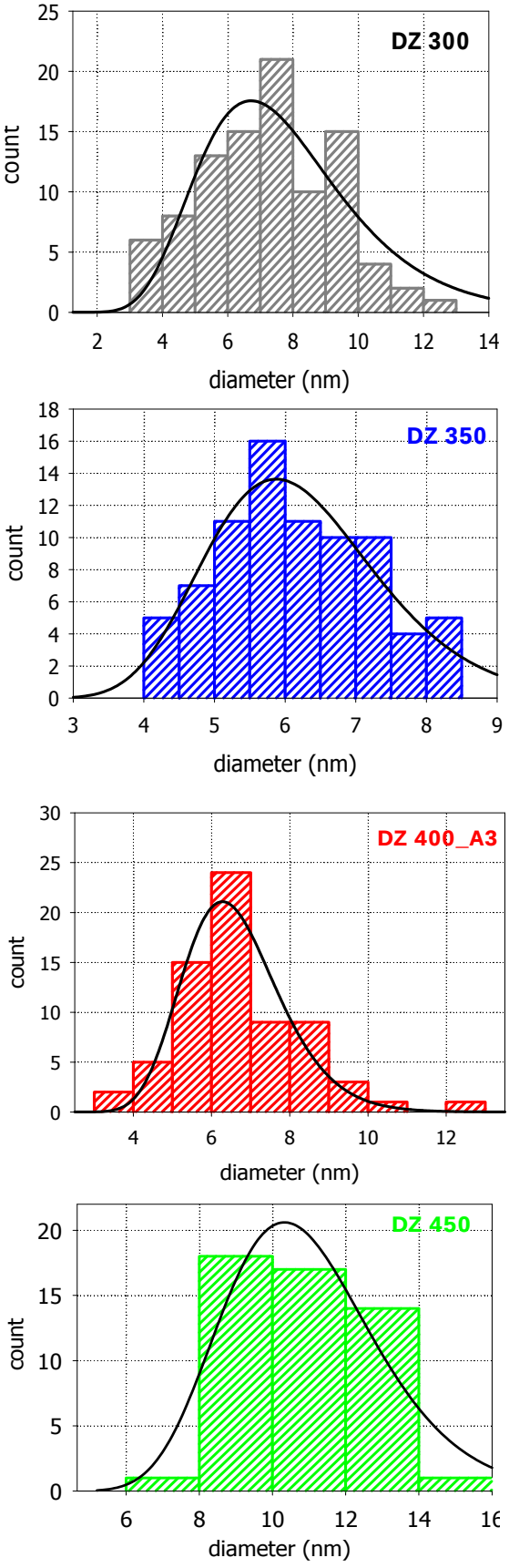

Figure 4.8. Histograms obtained from the TEM images fitted using the LogNormal distribution with its maxima belonging to the median size of particles.

4.3.2. HRTEM observation

The DZ 300 sample was characterized by HRTEM. Figure 4.9.(a) represents the high resolution image of one part of the sample having the crystalline NPs. We can follow the diffraction fringes which correspond to the interlayer distances in the $CoCr_2O_4$ structure. The interlayer distance was determined and the value of 2.5 Å corresponding to layer (3 1 1) of cobalt chromite spinel structure was obtained. Figure 4.9. (b) represents the electron diffraction pattern of selected area (SAED). The results from SAED are shown in Table 4.1. We can follow both diffused circles corresponding to amorphous part of the sample and white spots representing the diffraction from the crystallites. The SAED patterns confirm the presence of $CoCr_2O_4$ in the sample.

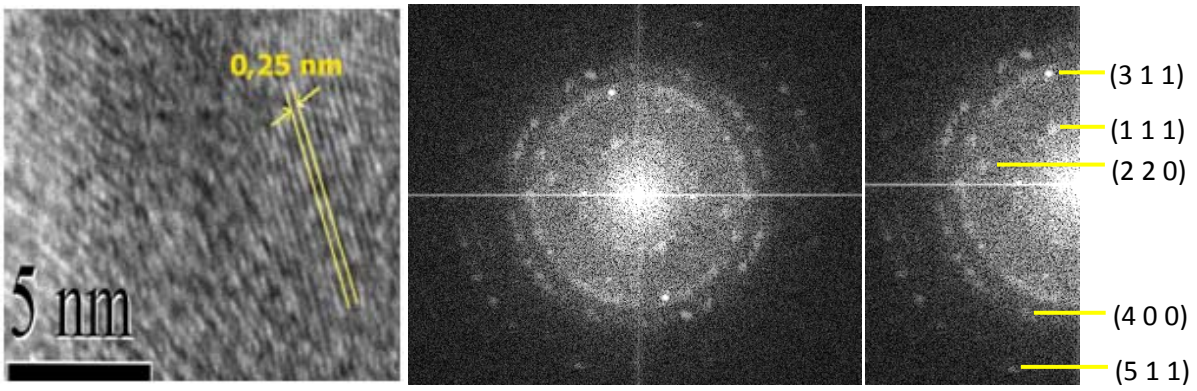

Figure 4.9. (a) HRTEM image and (b) SAED of the DZ 300 sample.

h k l	(1 1 1)	(2 2 0)	(3 1 1)	(4 0 0)	(5 1 1)
d_{hkl} (Å)	4.840	2.947	2.512	2.084	1.603

Table 4.1. Assignments of SAED image of the DZ 300 sample.

4.3.3. SEM observations

SEM technique is not suitable for the morphology characterization of the sample due to very small particle size and not sufficient resolution of SEM method. Nevertheless, the energy dispersed X-ray analysis (EDX) which is the part of SEM apparatus was used for the elemental analysis of the samples. This analysis confirmed us that the molar ratio between cobalt and chromium is equal to 1:2. The results are shown in the following Figure 4.10. and Table 4.2.

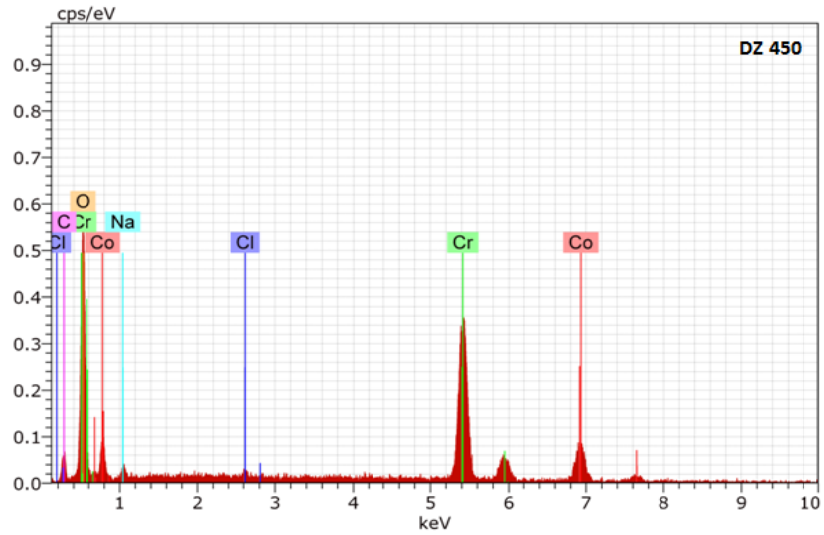

Figure 4.10. The EDX spectrum of the DZ 450 sample

Element	C Norm (wt%)	C Atom. (at. %)	Error (%)
Cobalt	28.53	18.19	1.1
Chromium	50.91	36.79	1.6
Oxygen	16.75	39.34	2.9
Chlorine	0.96	1.02	0.1
Sodium	2.85	4.65	0.3
Total	100.00	100.00	

Table 4.2.. The results of EDX analysis of the DZ 450 sample

4.4. Particle Size Determination

The particle size was determined from different characterization methods (TEM, PXRD) and using different approaches. Results are shown in Table 4.3. In the column “PXRD”, two types of size determination are shown. The first column corresponds to the determination using the Scherrer equation and the second column represents the particle size obtained from Rietveld analysis. In column “TEM”, the results from direct observation of particle size from TEM images are given. Column “LogNormal” then represents the values of median size obtained from LogNormal distribution. Column “Average” shows the average values of particle sizes taken from TEM images. In order to follow the influence of annealing temperature on the lattice parameter, we performed the calculation of unit cell dimension using FullProf program and the results are given in the last "a" column. The particle sizes obtained from TEM images are greater than those determined from PXRD. PXRD gives the particle sizes of the individual crystallites that form polycrystalline particle, while TEM gives us the shape and dimension of entire polycrystalline particle.

Sample	Annealing Temperature (°C)	PXRD		TEM images		a (Å)
		Scherrer (nm)	Rietveld (nm)	Median size (nm)	Average (nm)	
DZ 300	300	4.9 ± 1.4	4.4	6.9	7.2 ± 1.9	8.271
DZ 350	350	5.4 ± 1.3	5.1	5.9	6.2 ± 1.7	8.282
DZ 400	400	6.9 ± 3.2	6.2	6.4	6.8 ± 1.1	8.301
DZ 450	450	11.8 ± 1.4	11.5	11.5	12.0 ± 1.8	8.306

Table 4.3. Summary of the results determined from TEM and PXRD.

4.5. Thermogravimetry

In order to determine the content of organics and water in the samples, TG-DTA analysis was carried out. The all treated samples were analyzed. The TG-DTA curves of the annealed sample (DZ 300) are given in the Figure 4.11. It can be seen from TG curve of the DZ 300 sample that organics content is approximately 5 % and the organics removal and dehydration is completed at the temperature of 400 °C. The broad peak at the temperature of 220 °C corresponds to the endo-effect (decomposition of organics or dehydration) and the broad band at the temperature of 350 °C corresponds to the exo-effect.

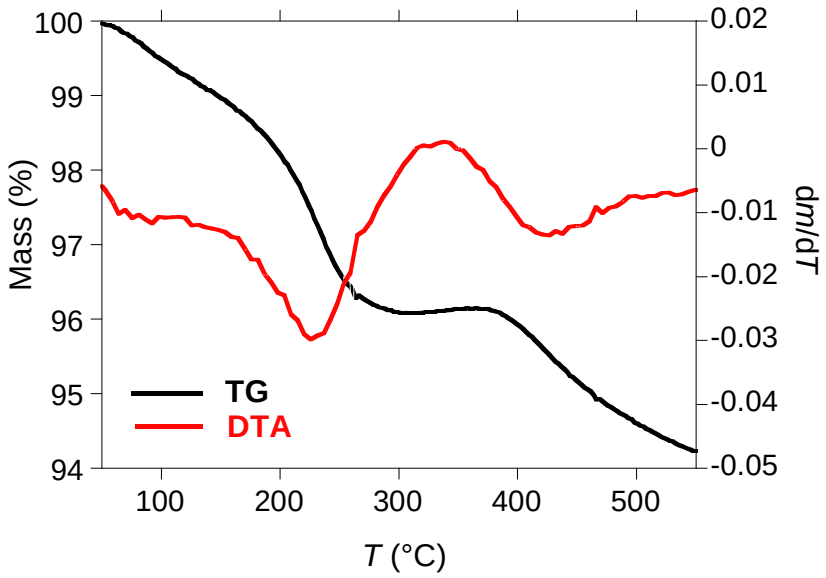

Figure 4.11. Thermogravimetric analysis of the samples DZ 300.

4.6. Magnetic Measurement

It was previously found[8] that the bulk $CoCr_2O_4$ (Figure 4.12.) is ferrimagnetically ordered below the Curie temperature of T_c = 94 K. It undergoes an additional order-to-order magnetic phase transition to a long-range spiral magnetic order at T_S = 27 K with an incommensurate propagation vector of (q q 0), (q = 0.63). The ground state magnetic order is established below the so called lock-in transition at around 15 K resulting in a net change of the q-value[18]. The above mentioned values are further used for interpretation of the magnetic measurements of the nanoparticles.

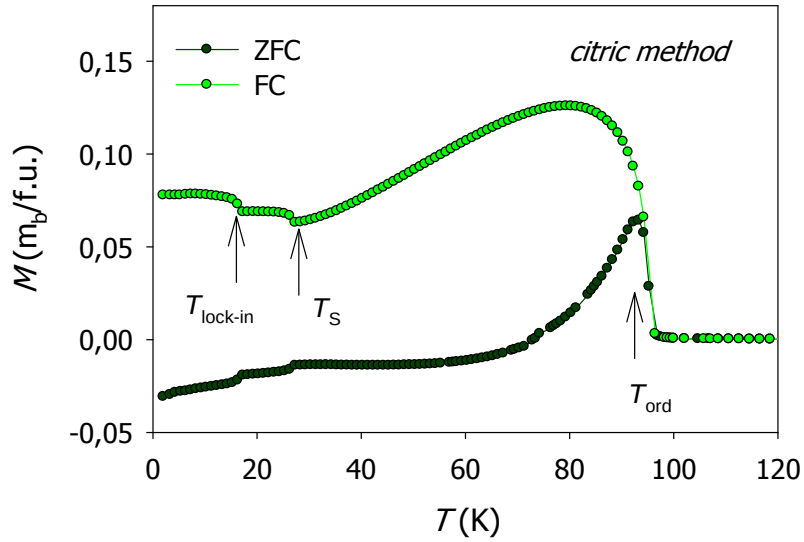

Figure 4.12. Temperature dependence of the zero-field (ZFC) and field-cooled (FC) magnetization, M at B = 0.05 T of the bulk (reference) sample prepared by the citric method.

Magnetic properties of the prepared $CoCr_2O_4$ nanoparticles were studied using SQUID magnetometer. Results of the magnetic measurements are shown in Figures 4.13 − 4.17. The zero-field cooled (ZFC) and field cooled (FC) curves exhibit glassy-like behaviour with the furcation temperatures, T_f, as summarized in Table 4.4. Comparing the value of T_f with the bulk one, the shift towards lower temperatures can be observed. The continuous collapse of the long-range magnetic order with decreasing particle size can be explained by the fact that the size of the nanoparticles is comparable to the correlation length of the spiral component in the ground state of the magnetic structure of bulk $CoCr_2O_4$ (3.1 nm)[20].

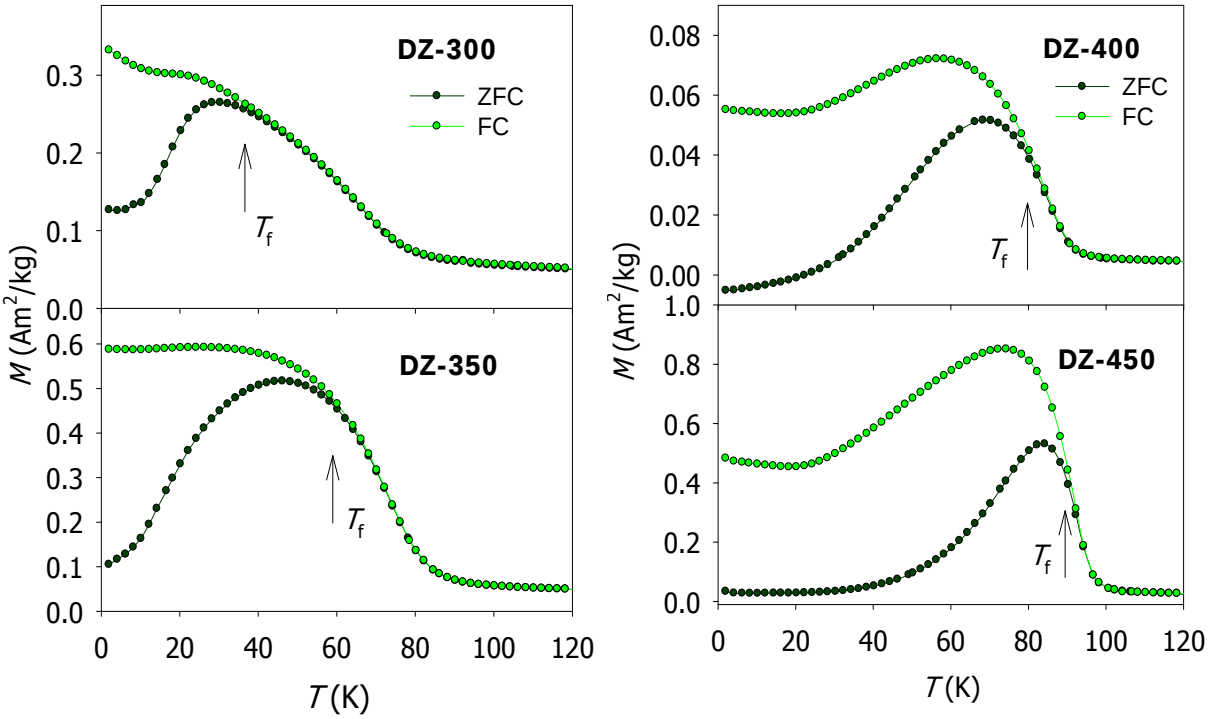

Figure 4.13. Temperature dependencies of the zero-field cooled (ZFC) and field-cooled (FC) magnetization, M of the DZ 300, DZ 350, DZ 400_A3, DZ 450 samples (B = 0.01 T).

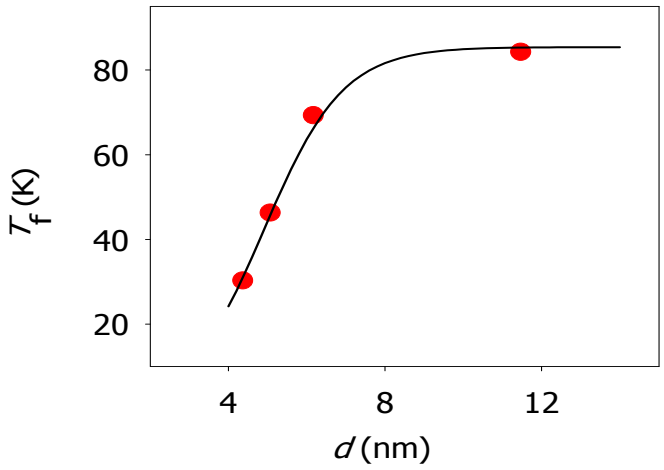

Figure 4.14. Evolution of the furcation (freezing) temperature, T_f with respect to the particles size.

The typical magnetization isotherms recorded above the T_c, between the T_c and the T_s, and under the T_s, respectively, of the DZ 400_A3 sample is shown in the Figure 4.15. The magnetization curve carried out at 300 K show linear dependence on the applied field without hysteresis. This behaviour is generally characteristic for paramagnetic phases. In fact, no hysteresis is observed for the measurements carried out at the temperatures higher than

50 K. The magnetization isotherm measured at 2K already shows the hysteresis, but the magnetization does not reach the saturation even in the field of 7 T. The lack of saturation can be attributed either to the spin disorder, which can be observed at the surface of nanoparticles[21], or it can be rather explained by the formation of the glassy-like state in small particles. The hysteresis loops exhibit a moderate coercive field; the values are given in the Table 4.4. The values of the coercivity, H_c of our sample are larger than it was reported in literature for a single crystal (~ 50 Oe)[20]. This effect has no straightforward interpretation using the concept of superparamagnetism, as the bulk magnetic structure is complex and the ordering temperatures are rather low. The enhancement of the coercivity can be observed in non-stoichiometric samples or in samples containing a small amount of the CoO or Cr_2O_3 (not detectable by PXRD) which can be involved in the exchange-bias phenomena. Considering a collective spin-glass-like state, the increase of the coercivity is also expected.

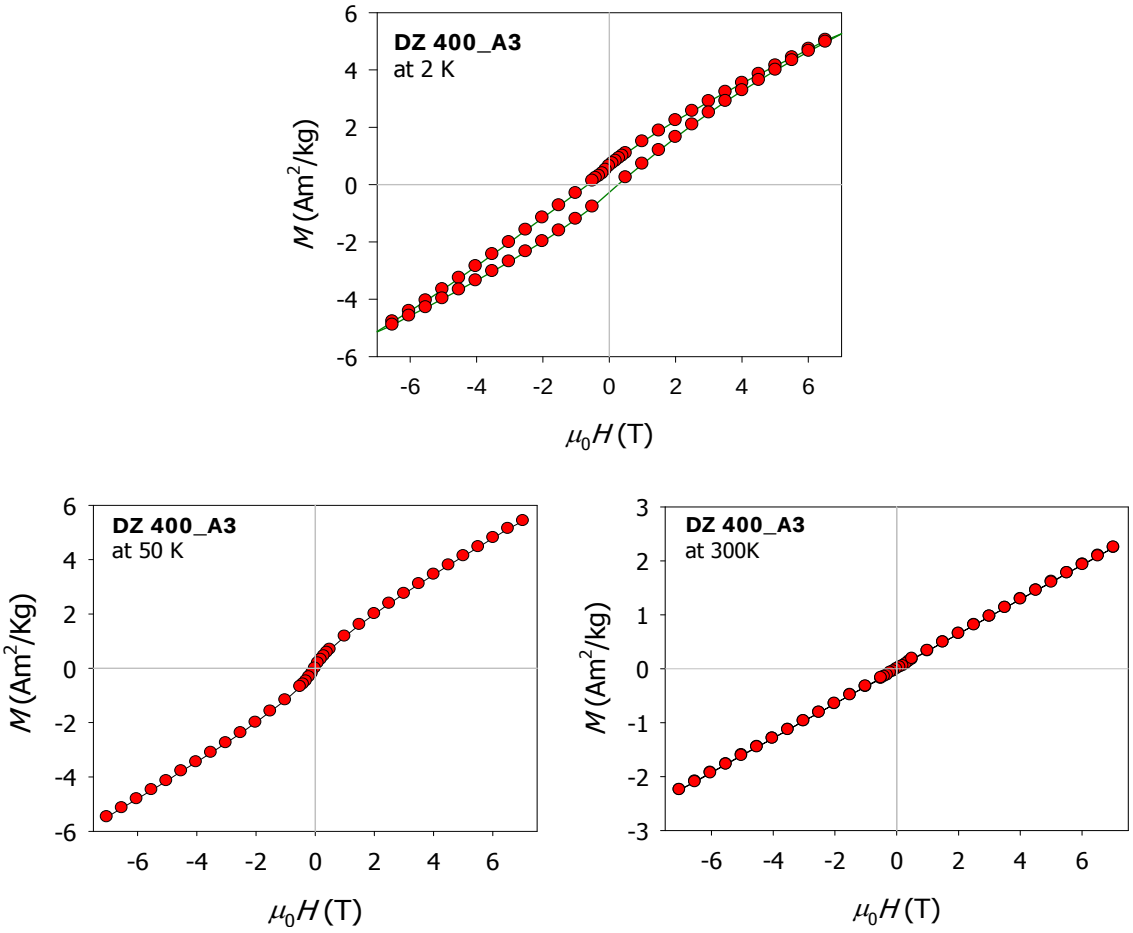

Figure 4.15. Hysteresis loops of DZ 400_A3 sample recorded at the temperature 2 K, 50 K and 300 K.

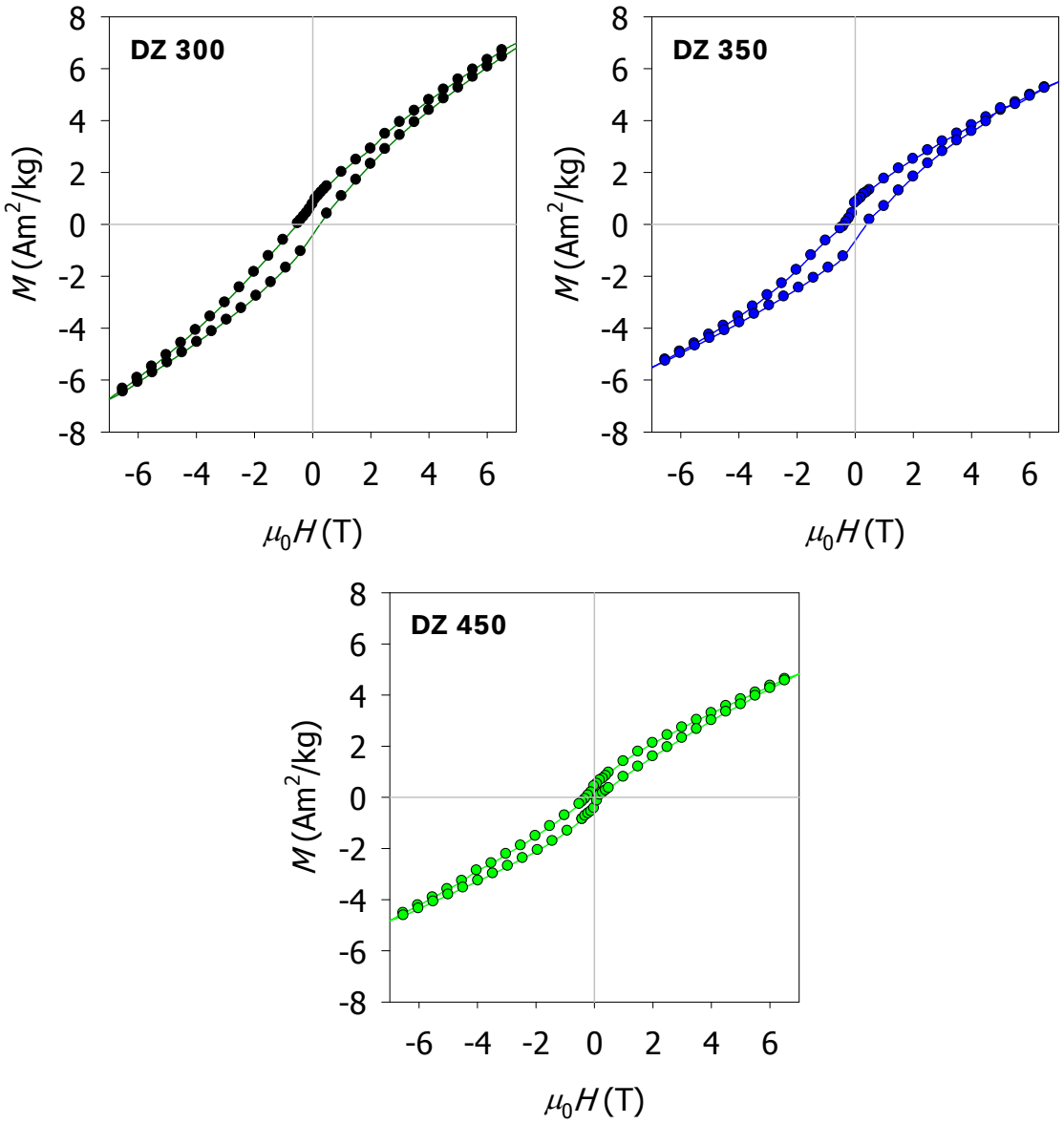

Figure 4.16. Hysteresis loops of DZ 300, DZ 350 and DZ 450 recorded at the temperature of 2 K.

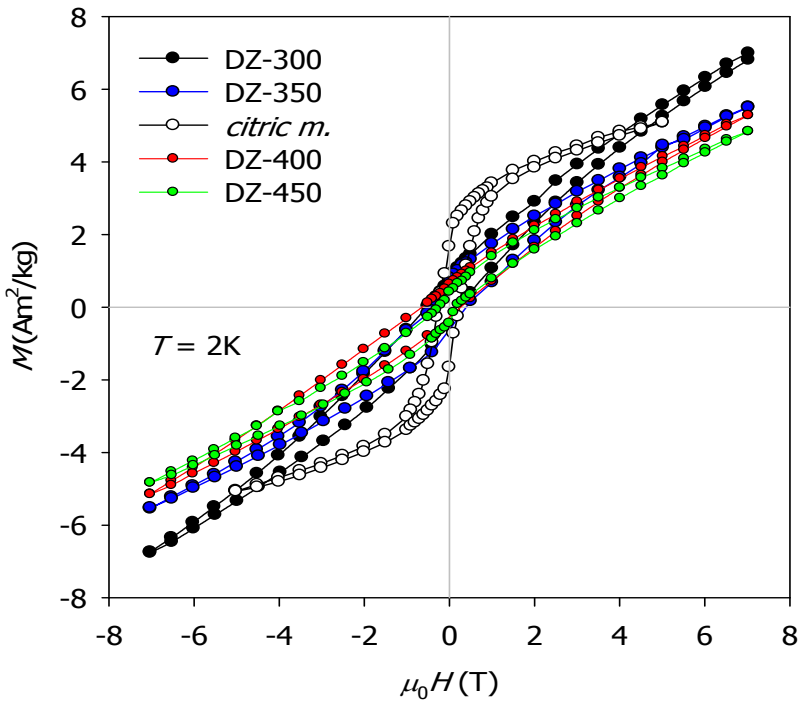

Figure 4.17. Hysteresis loops of the annealed samples in the comparison with the bulk sample recorded at 2 K.

Sample	T_f (K)	$\mu_0 Hc$ (T)
DZ 300	30	0.4014
DZ 350	46	0.2018
DZ 400_A3	69	0.5027
DZ 450	84	0.1009

Table 4.4. Summary of the results of the magnetic measurements: freezing temperature, T_f and coercivity, H_c of the prepared samples.

4.7. Raman and Infrared Spectroscopy

The $CoCr_2O_4$ belongs to the space group $Fd\bar{3}m$. The atoms of $CoCr_2O_4$ occupy 8a (tetrahedral), 16d (octahedral) and 32e (oxygen) Wyckoff sites. These sites contribute to $F_{2g} + F_{1u}$, $A_{2u} + E_u + F_{2u} + 2F_{1u}$ and $A_{1g} + E_g + 2F_{2g} + F_{1g} + A_{2u} + E_u + F_{2u} + 2F_{1u}$ modes[23]. From this modes, the A_{1g}, F_{2g} and E_g are active in Raman. From the prediction of the selection rules it was concluded that Raman spectra consist of 5 bands ($A_{1g} + E_g + 3\ F_{2g}$), which were found in the bulk sample (Figure 4.18).

The samples were measured in the spectral range of 100 - 2000 cm^{-1}. The Raman spectra of the samples are shown in Figure 4.19. 5 bands were found and in addition of these bands, the broad bands were observed in the DZ 300 and DZ 350 samples. This is probably due to the small particle size. The position of 5 bands of the samples is shown in Table 4.3.

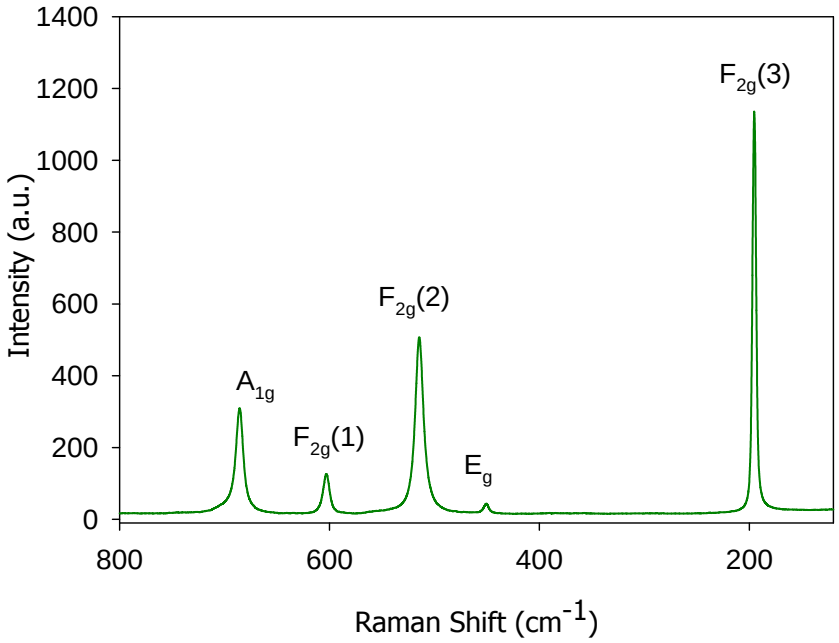

Figure 4.18. Raman spectrum of the bulk sample, which was prepared by sol-gel method using the propylene oxide as gelation agent.

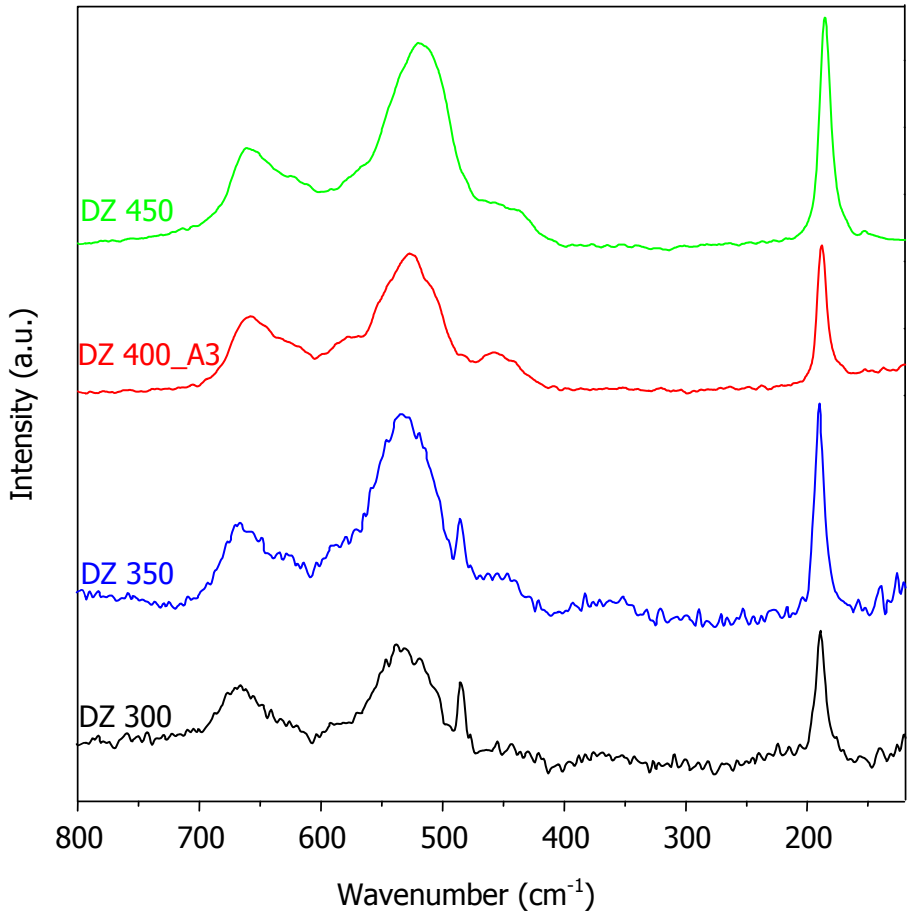

Figure 4.19. Raman spectra of $CoCr_2O_4$ samples.

Raman shift (cm^{-1})					
DZ 300	**DZ 350**	**DZ 400_A3**	**DZ 450**	**Bond vibration**	**Symmetry**
190	190	190	186	δ (O - Co - O)	F_{2g} (3)
484	484	458	454	$\upsilon_s(Cr-O)+\upsilon_S\,(Co-O)$	E_g
534	534	523	519	$\upsilon\,(Cr-O)$	F_{2g} (2)
631	631	628	622	$\upsilon_s(Cr-O)$	F_{2g} (1)
669	665	660	658	$\upsilon_s(Cr-O)$	A_{1g}

Table 4.5. Interpretation of the $CoCr_2O_4$ Raman spectra.

Further characterization was carried out by IR spectroscopy. It was found in the previous work by Preudhomme[24] that in the bulk chromite samples, there are four F_{1u} modes, which are active in infrared spectra ($F_{1u}(\upsilon_4) = 200\ cm^{-1}$, $F_{1u}(\upsilon_3) = 380\ cm^{-1}$, $F_{1u}(\upsilon_2) = 530\ cm^{-1}$, and $F_{1u}(\upsilon_1) = 630\ cm^{-1}$). Figure 4.20. represents the IR spectrum of bulk $CoCr_2O_4$ which was prepared by sol-gel method and measured in the range of 450 - 800 cm^{-1} for the comparison with cobalt chromite nanoparticles IR spectra. From this Figure, we can observe two broad bands having fine structure. The peaks located at 610 cm^{-1}, 631 cm^{-1}, and 670 cm^{-1} belong to asymmetric bond vibration of υ_1 ($Cr - O$) and two peaks of 492 cm^{-1} and 530 cm^{-1} belong to bond vibration ofυ_2 ($Cr - O$). This fine structure has not yet been interpreted but it was found that it strongly depends on many parameters like synthesis conditions, etc.[24] and it probably reflects the different distribution of cations (Co^{2+}, Cr^{3+}) in tetrahedral and octahedral sites.

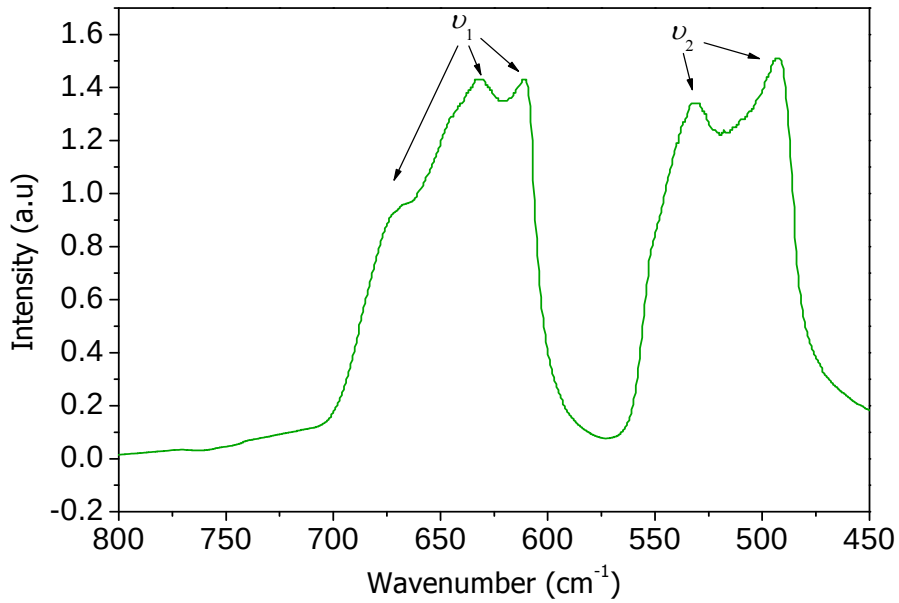

Figure 4.20. The infrared spectra of bulk sample, which was prepared by sol-gel method using propylene oxide as gelation agent.

Figure 4.21. shows the IR spectra of nanocrystalline $CoCr_2O_4$ (DZ 400_A3 sample). In the comparison with the bulk analogue, we obtained similar spectrum with two broad bands located around 630 cm^{-1} (υ_1) and 520 cm^{-1} (υ_2). The fine structure of these bands is not so sharp, which is probably due to the nanosize dimensions of this sample. Nevertheless, we can

state that infrared spectroscopy represents another method which can confirm us the spinel structure of cobalt chromite nanoparticles.

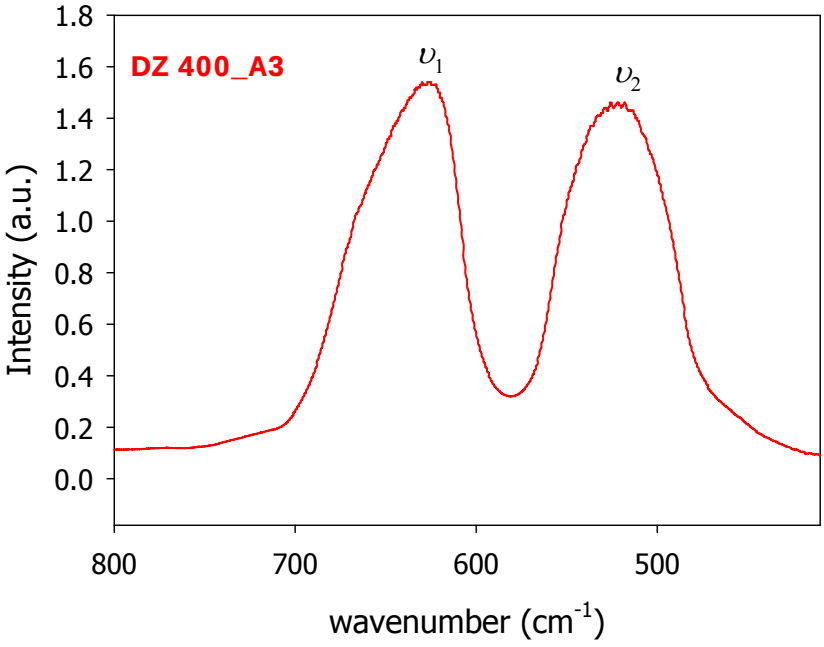

Figure 4.21. The Infrared spectra of the DZ 400_A3 sample.

Chapter 5

Conclusion

The hydrothermal method in oleic acid – sodium oleate – water – ethanol was successfully used for the preparation of cobalt chromite nanoparticles with the size ranging from 3 to 16 nm, yielding the as-prepared nanoparticles capped by the oleic acid. The mechanism of the formation of the nanoparticles in the oleic acid - sodium oleate - water system was also proposed. The content of the organic phase was determined by the thermogravimetric analysis; the as-prepared particles contain ~ 5 %, respectively. The nanoparticles were further characterized by Powder X-ray Diffraction, Electron microscopy (TEM, HRTEM, SEM), Raman and FTIR Spectroscopy and magnetic measurements.

The EDX analysis revealed that the prepared nanoparticles have the molar ratio of Co:Cr = 1:2, which corresponds to the theoretical stoichiometric ratio of the cobalt chromite with the spinel structure.

The particle sizes were determined from the PXRD and EM using various procedures. It was found that the particles size increases with the increasing annealing temperature, as expected. The particle size distribution, determined from the TEM analysis is relatively narrow. The particle sizes determined from TEM is slightly larger than that ones determined by PXRD, what is in the good agreement with the expected behaviour.

The magnetic measurements of the nanoparticles with the size below 16 nm show typical features of the glassy-like behaviour with a furcation temperature, T_f, as it is evidenced by the temperature dependence of the zero-field cooled (ZFC) and field-cooled (FC) magnetization recorded in low magnetic fields. The values of the T_f shifts towards lower temperatures with the decreasing particle size. The collapse of the magnetic ordering in the samples with particle size below 16 nm can be explained by the fact that the size of the nanoparticles is of the same order as the coherence length of the spin wave in the ground state magnetic structure.

References

[1] S. Sun, H. Zeng, D. B. Robinson, S. Raoux, P. M. Rice, S. X. Wang, G. Li, *Monodisperse* MFe_2O_4 (M = Fe, Co, Mn) *Nanoparticles,* JACS Articles **2004**, 4, 126–132.

[2] X. Wang, J. Zhuang, Q. Peng, Y. Li, *A General Strategy for Nanocrystal synthesis,* Nature **2005**, *437*, 121–4.

[3] Ch. Kittel, *Introduction to Solid State Physics- 7th ed.,* **1996**.

[4] W. D. Callister, *Fundamentals of Materials Science and Engineering*, **2001**.

[5] N. Majlis, *The Quantum Theory of Magnetism*, World Scientific Publishing Co. Pte. Ltd., **2000**.

[6] S.Blundell, *Magnetism in Condensed Matter*, **2004**.

[7] A. Beiser, *Úvod do Moderní Fyziky,* Academia, Praha, **1975.**

[8] Y. Yamasaki, S. Miyasaka, Y. Kaneko, J.-P. He, T. Arima, Y. Tokura, *Magnetic Reversal of the Ferroelectric Polarization in Multiferroic Spinel Oxide,* Physical Review Letters **2006**, *96*, 207204.

[9] H. Katsura, N. Nagaosa, A. V. Balatsky, *Spin Current and Magnetoelectric Effect in Noncollinear Magnets,* Physical Review Letters **2005**, *95*, 057205.

[10] K. Dwight, *Ferrimagnetic Spiral Configurations in Cobalt Chromite* Le Journal de Physique **1964**, 528–536.

[11] K. Tomiyasu, J. Fukunaga, H. Suzuki, *Magnetic short-range order and reentant-spin-glass-like behaviour in* $CoCr_2O_4$ *and* $MnCr_2O_4$ *by means of neutron scattering and magnetization measurements,* Physical Review B **2004**, *70*, 214434.

[12] K. Tomiyasu, K. Kamazawa, *Neutron Scattering Study of* $CoCr_2O_4$*,* Physica B: Condensed Matter **2007**, *392*, 16–19.

[13] D. P. Dutta, J. Manjanna, a. K. Tyagi, *Magnetic Properties of Sonochemically synthetized* $CoCr_2O_4$ *Nanoparticles,* Journal of Applied Physics **2009**, *106*, 043915.

[14] C. Rath, P. Mohanty, *Magnetic Properties of Nanoparticles of Cobalt Chromite,* Journal of Superconductivity and Novel Magnetism **2010**, *24*, 629–633.

[15] C. Rath, P. Mohanty, a. Banerjee, *Magnetic Phase Transition in Cobalt Chromite Nanoparticles,* Journal of Magnetism and Magnetic Materials **2011**, *323*, 1698–1702.

[16] M. Edrissi, A. R. Keshavarz, *Synthesis of Cobalt Chromite Nanoparticles by Thermolysis of Mixed Cr^{3+} and Co^{2+} Chelates of 2-Mercaptopyridin N-Oxide,* Nano-Microletters **2012**, *4*, 83–89.

[17] S. K. Durrani, S. Z. Hussain, K. Saeed, *Hydrothermal Synthesis and Characterization of Nanosized Transition Metal Chromite Spinels,* Journal of Turkish Chemistry **2012**, *36*, 111–120.

[18] L. J. Chang, D. J. Huang, W.-H. Li, S.-W. Cheong, W. Ratcliff, J. W. Lynn, *Crossover from incommensurate to commensurate magnetic orderings in $CoCr_2O_4$,* Journal of physics: Condensed matter **2009**, *21*, 456008.

[19] J. Rodríguez-Carvajal, *An Introduction to the Program FullProf,* L. L. B. Cea-cnrs **2001**.

[20] K. Tomiyasu, J. Fukunaga, H. Suzuki, *Magnetic short-range order and reentrant-spin-glass-like behaviour in $CoCr_2O_4$ and $MnCr_2O_4$ by means of neutron scattering and magnetization measurements,* Physical Review B **2004**, *70*, 214434.

[21] R. H. Kodama, a. E. Berkowitz, E. J. McNiff, S. Foner, *Surface spin disordere in ferrite nanoparticles,* Journal of Applied Physics **1997**, *81*, 5552.

[22] J.M.D. Coey, *Noncollinear Spin Arrangement in Ultrafine Ferrimagnetic Crystallites,* Physicals rewiew letters, **1971**, *27*, 1970–1972.

[23] K. E. Sickafus, J. M. Wills, N. W. Grimes, *Spinel Compounds: Structure and Property Relations*, Journal of the American Ceramic Society, **1999**, *82*, 3279–92.

[24] J. Preudhomme, P. Tarte, *Infrared Studies of Spinel-III The normal II-III spinels,* Spectrochimica Acta, **1971**, 27, 1817–1835.

Abbreviations

CGS	centimeter, gram, second (old unit system)
SI	International System of Units
NPS	Nanoparticles
LSS	Liquid-Solid-Solution
TG	Thermogravimetry
DTA	Differential thermal analysis
FTIR	Fourier Transform Infrared Spectroscopy
NIR	Near infrared
PDI	Polydispersity index
EM	Electron Microscopy
TEM	Transmission Electron Microscopy
HRTEM	High Resolution Transmission Electron Microscopy
SEM	Scanning Electron Microscopy
EDX	Electron Dispersed X-ray analysis
SAED	Selected Area Electron Diffraction
PXRD	Powder X-ray Diffraction
FWHM	Full width at half maximum
ZFC	Zero field cooled
FC	Field cooled
IR	Infrared
SPM	Superparamagnet
SFM	Superferromagnet
SSG	Super-spin glass
SSG-like system	Super-spin glass like system
RKKY	Ruderman-Kittel-Kasuya-Yosida

Attachment

Presentations

Conference:

7th Interregional Workshop on Advanced Nanomaterials (IWAN), Wroclaw, Poland, 12 − 13 November 2011, poster:

Hydrothermal preparation of cobalt chromite nanoparticles

Dominika Zákutná[1], Daniel Nižňanský[1], Anton Repko[1], Jana Poltierová-Vejpravová[2]

[1]Department of Inorganic Chemistry Faculty of Sciences, Charles University, 128 43 Prague 2, Czech Republic

[2]Institut of Physics, Academy of Sciences of Czech Republic v.v.i, Department of Functional Materials Magnetism of Nanosystems Group, Na Slovance 2, 182 21 − Prague 8 Czech Republic

Abstract

Cobalt chromite is a potential multiferroic material. Nanoparticles were prepared by hydrothermal method. Cobalt and chromium oleates were used for the preparation. They were dissolved in the system water-ethanol and treated at 200 °C. As prepared product was amorphous. Then, precipitate was heat treated in a furnace at different temperatures up to 500 °C. The resulting samples were characterized X-Ray Diffraction, TEM and magnetic measurement. The sample heat treated at 300 °C was already crystalline. The mean particles size determined by Scherrer equation was 10 nm. This is in agreement with the TEM observation.

Keywords: oleates; X-Ray diffraction; $CoCr_2O_4$; magnetic properties;

Acknowledgment

The work was supported by the Grant Agency of the Czech Republic under project no. P108/10/1250.

Conference:

Joint European Magnetic Symposia, Parma, Italy, 9 – 14 September 2012, poster: Magnetic Properties of Cobalt Chromite Nanoparticles

Magnetic Properties of Cobalt Chromite Nanoparticles

Dominika Zákutná[1,2], Daniel Nižňanský[1], Anton Repko[1], Jana Vejpravová[2], Carla Cannas[3]

[1]Department of Inorganic Chemistry Faculty of Sciences, Charles University, 128 43 Prague 2, Czech Republic,

[2]Institut of Physics, Academy of Sciences of Czech Republic v.v.i, Department of Functional Materials Magnetism of Nanosystems Group, Na Slovance 2, 182 21 − Prague 8 Czech Republic,

[3]Università di Cagliari, Dipartimento di Scienze Chimiche, Complesso, Universitario di Monserrato, 09042 Monserrato (CA), Italy

The multiferroic $CoCr_2O_4$ with no orbital degrees of freedom shows tiny deviations from cubic structure, even in its ground state. It orders ferrimagnetically below the Curie temperature, T_C =94 K, and an additional order-to-order magnetic phase transition to spiral magnetic phase occurs at T_S = 27 K. Magnetocapacitive measurements show that the dielectric constant of $CoCr_2O_4$ couples to the spiral magnetic order parameter, but is insensitive to the ferrimagnetic spin component. In our work, we address size effect magnetic properties of $CoCr_2O_4$ nanoparticles.

The nanoparticles (NPs) of cobalt chromite ($CoCr_2O_4$) were synthesized by hydrothermal method, and subsequently annealed from 300 °C to 500°C. The crystal structure and particle size distribution of the NPs were investigated by powder Xray diffraction (XRD), dynamic light scattering (DLS) and transmission electron microscopy (TEM). The particle size was found to be about 5-20 nm for the samples annealed from 300 °C to 500 °C according to the TEM image. The TEM image also showed the particles were synthesized nearly spherical crystal shape.

Magnetization vs. temperature measurements revealed a transition from paramagnetic to superparamagnetic (SPM) state in contrast with the transition from paramagnetic to long range ferrimagnetic state reported in bulk samples. The zero-field cooled (ZFC) and field-

cooled (FC) curves show glassy-like behaviour with furcation temperature, T_f = 38 K. The hysteresis loops exhibit a moderate hysteresis ($\mu_0 \cdot H_c \sim 0.4$ T) and no trend to saturation up to 7T, in contrast to the bulk sample. The typical features of the $CoCr_2O_4$ magnetic order are suppressed in the nanoparticles, resulting in a (super)spin-glass like state.

Conference:

8th Interregional Workshop on Advanced Nanomaterials (IWAN), Franktfurt n. O., Germany, 12 − 13 November 2012, oral: Preparation and Characterization of Cobalt Chromite Nanoparticles.

Preparation and Characterization of Cobalt Chromite Nanoparticles

Dominika Zákutná[1,2], Daniel Nižňanský[1], Anton Repko[1], Andrea Ardu[3], Carla Cannas[3], Jana Vejpravová[2]

[1]Department of Inorganic Chemistry Faculty of Sciences, Charles University, 128 43 Prague 2, Czech Republic,

[2]Institut of Physics, Academy of Sciences of Czech Republic v.v.i, Department of Functional Materials Magnetism of Nanosystems Group, Na Slovance 2, 182 21 − Prague 8 Czech Republic,

[3]Università di Cagliari, Dipartimento di Scienze Chimiche, Complesso, Universitario di Monserrato, 09042 Monserrato (CA), Italy

Abstract

The $CoCr_2O_4$ nanoparticles (NPs) were prepared by hydrothermal treatment of chromium and cobalt oleates in a mixture of solvents composed of water, ethanol or pentanol at various temperatures. Samples, which were prepared by hydrothermal treatment at 200 °C, were amorphous. Therefore these samples were subsequently annealed on air at temperatures from 300 °C to 500 °C. The aim of the work is to prepare the well isolated uniform nanoparticles, and to address size effect in magnetic properties of the $CoCr_2O_4$ nanoparticles of various sizes.

The obtained NPs were characterized by X-ray diffraction (XRD), transmission electron microscopy (TEM), scanning electron microscopy (SEM), Raman and infrared spectroscopy

(FTIR), dynamic light scattering (DLS) and magnetic measurements. The particle size distribution was investigated by XRD and TEM.

The XRD vibration spectroscopy experiments confirmed that the samples are composed of single phase $CoCr_2O_4$. According to the TEM images, the NPs size was found to be in the range of 2-20 nm, depending on the annealing temperature. The TEM images also showed that the particles had the tendency to form the aggregates during the annealing. The particles, which were prepared by hydrothermal treatment at temperature higher than 200 °C, have nearly spherical shape.

Magnetization vs. temperature measurements revealed the transition from paramagnetic to superparamagnetic (SPM) state in contrast with the transition from paramagnetic to long range ferrimagnetic state reported in bulk samples. The hysteresis loops exhibits a moderate hysteresis ($\mu_0 \cdot H_c \sim 0.4$ T) and no trend to saturation up to 7 T. The zero-field cooled (ZFC) and field cooled (FC) curves show glassy-like behaviour. The typical features of the magnetic order of cobalt chromite are suppressed in the nanoparticles, resulting in a (super)spin-glass like state.

Keywords: oleates; XRD; TEM, $CoCr_2O_4$; magnetic properties;